Chapter 2
Earthquake-Resistant Design and Reinforcement

Abstract For the methods of earthquake resistant design of structures, firstly the seismic coefficient method and the modified seismic coefficient method in which the response spectra are used, are explained, and the development of the design methods against soil liquefaction as well as long period components of earthquake ground motion are introduced.

The new concept for earthquake resistant design against two levels of ground motion, and the revisions of the design codes and standards after the 1995 Kobe earthquake are described. Furthermore, theory on S-wave propagation and the characteristics on the response of the surface ground, amplification of ground motion and dominant period are explained. The mass-spring model is explained to solve the dynamic response of surface ground.

In addition, the design procedure of nuclear power plant and tsunami-resistant measures after the 2011 Tohoku earthquake are introduced. Furthermore, technologies of reinforcement of existing structures are introduced.

Keywords Earthquake-resistant design • Mass-spring model • Nuclear power plant • Response spectrum • Seismic wave propagation • Tsunami

2.1 Beginning of Earthquake-Resistant Design in Japan

2.1.1 Earthquake Engineering and Seismology

The difference between earthquake engineering and seismology might be difficult to understand for non-professional people outside these fields. Characteristics of active faults that cause earthquakes and propagation of seismic waves in the earth crust are investigated in seismology, and are illustrated in Fig. 2.1. One of the major objectives of seismology is earthquake prediction. As seen in the 2011 Tohoku earthquake (Great East Japan Earthquake and Tsunami Disaster), seismology was completely unable to predict an earthquake of $M_{JMA} = 9.0$ (magnitude on the

M. Hamada, *Engineering for Earthquake Disaster Mitigation*,
Springer Series in Geomechanics and Geoengineering,
DOI 10.1007/978-4-431-54892-8_2, © Springer Japan 2014

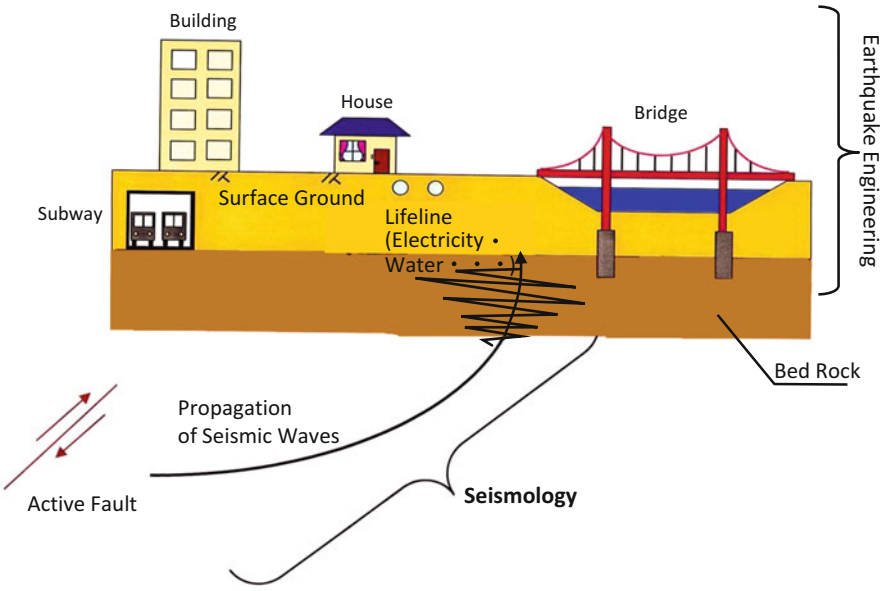

Fig. 2.1 Earthquake engineering and seismology

Japan Metrological Agency scale). Therefore, whether earthquake prediction will be able to significantly contribute to mitigation of earthquake disasters in the next several decades is very questionable, because problems may persist. A thorough examination of the failure of prediction of the 2011 Tohoku earthquake are indispensable. Without this endeavor, there should be no expectation of new developments in earthquake prediction in our country. Furthermore, it is very important to explain to people that short-period earthquake prediction from 1 day to several weeks before an earthquake will be impossible.

The purpose of earthquake engineering is to analyze the response of structures such as buildings, bridges and surface ground to earthquake motions, and ensure their safety. The ultimate goal of this engineering is to create safer and more secure societies, based on the design and construction of structures.

Originally, the seismology discipline was developed by scientific researchers engaged in studies such as geophysics. In contrast, earthquake engineering is peopled by civil engineering, mechanical engineering, geological engineering, and related fields.

In the scientific field, researchers are asked to make predictions of earthquake probability and severity. In the engineering field, researchers are tasked with preventing loss of life and property by ensuring the safety of structures during future earthquakes and the tsunamis they induce. If both seismologic science and earthquake engineering execute their individual obligations and collaborative roles, a safe and risk-free society in the face of earthquakes and tsunamis would be achieved. However, it is a matter of regret that the activities of both fields have never been fully in cooperation, and that this was one of the principal causes of the great disaster of the Tohoku earthquake and tsunami.

Fig. 2.2 Damage to modernistic buildings by 1923 Kanto earthquake (home page of the National Science Museum)

2.1.2 Beginning of Earthquake-Resistant Design: Seismic Coefficient Method

Attention has been paid to earthquake-resistance of structures such as buildings and bridges, particularly since the 1923 Kanto earthquake (Great Kanto Earthquake Disaster), More than 576,000 houses and buildings were destroyed and burnt by the earthquake. Because of fires after the earthquake, there were more than 140,000 dead and missing. This earthquake has been regarded as the most serious calamity in modern history in Japan. Modernistic buildings constructed by European and American technologies during the Meiji Era (1868–1912) were greatly damaged in this event, as shown by Fig. 2.2.

In 1917, 6 years before the Great Kanto earthquake, Sano had proposed so-called seismic coefficient method to enhance the earthquake resistance of structures [1]. Figure 2.3 explains the concept of this method, where inertia force caused by earthquake motion is taken into the consideration for the design of structures, with addition of the self weight W. The inertia force H acting horizontally on the structures is obtained by W multiplied by horizontal seismic intensity coefficient K_H. That is, H is set to several tens of percent of W to examine building stability and the stress on individual members of buildings.

$$H = K_H \cdot W \tag{2.1}$$

One of subjects to apply the seismic coefficient method to actual design, is how to determine the horizontal seismic intensity coefficient. At the beginning of the adoption of this methods, about 10 % of the structure weight W, namely $K_H \fallingdotseq 0.1$,

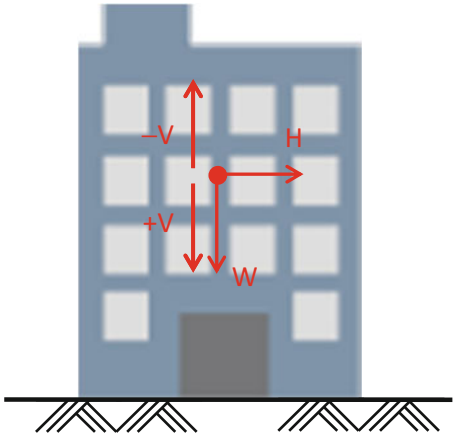

Fig. 2.3 Earthquake resistant design by the seismic coefficient method

was considered as the horizontal force. However, importance of the structures, impact of destruction of structures and other influential factors on society came to be considered later. Thus, larger values coefficient of seismic intensity gradually came to be adopted. Current horizontal seismic intensity coefficients in Japan are roughly shown below.

Ordinary buildings/bridges ≒ 0.2
Oil and petrochemical products ≒ 0.3 to 0.6
Dams ≒ 0.15
Port and harbor facilities ≒ 0.15 to 0.20
Nuclear power structures = 0.2 ∼ 0.6

As shown above, the seismic coefficient greatly depends on the type of structure. This is because characteristics of the dynamic response to earthquake motions and the importance of structures are, as stated above, under consideration.

The horizontal force H is the inertia force caused by an earthquake that acts on structures, therefore can be expressed as,

$$H = \alpha_m \cdot M \tag{2.2}$$

where α_m is the maximum horizontal acceleration on the structures by earthquake ground motion, and M is their mass. Eq. (2.2) can be rewritten as

$$H = \frac{\alpha_m}{g} \cdot M \cdot g \tag{2.3}$$

where g is gravitational acceleration (980 cm/s^2) and $M \cdot g$ the weight W of the structures. From Eqs. (2.1) and (2.3), the following can be obtained:

$$K_H = \frac{\alpha_m}{g} \tag{2.4}$$

that is, horizontal seismic intensity coefficient K_H is the ratio of the horizontal maximum acceleration acting on the structures to gravitational acceleration.

In addition to the horizontal force, earthquake-resistant design is often done with consideration of the inertia force V caused by acceleration in the vertical direction:

$$V = \pm K_V \cdot W \tag{2.5}$$

With respect to stability of structures and stress of members, the vertical force is acted in danger side direction, i.e., upward or downward. For the seismic coefficient intensity in the vertical, approximately 1/2 the horizontal seismic intensity coefficient is often used. K_V is called the vertical seismic intensity coefficient. In some cases, coefficients K_H and K_V are called engineering-oriented seismic intensity, for distinguishing them from the JMA seismic intensity and MMI (Modified Mercalli Intensity).

In earthquake-resistant design by the seismic coefficient method, the seismic forces are constantly acted in same direction. This implies that a static external force is considered. The inertia force by earthquake motion is dynamic, repetitively changing its direction with time. Comparing with the design in which repetitive loading is considered, design by a static external force in one direction generally has a superfluity of earthquake resistance of structures. Exact evaluations of such superfluity of structures designed with static seismic force compared with the repetitive load vary with dynamic characteristics and the failure process of structures. Large shaking-table tests and numerical analysis have been conducted to clarify the behavior of that failure process, toward evaluating the superfluity. However, it is generally difficult to pursue the failure process using an experimental model of reduced scale, because the similitude requirement is not satisfied because of strong non-linearity between external force and structural deformation in the failure process. Full-size (same size as actual structures) models are needed. Therefore, a three-dimensional and actual-size experimental facility (E-Defence) was constructed in Miki, Hyogo Prefecture after the 1995 Kobe earthquake [2]. The facility has a large shaking table with loading capacity 1,200 tf. With the aid of this facility, failure experiments have been conducted for reinforced concrete buildings, and pile foundations. Thus, research on the failure process is underway.

2.1.3 Modified Seismic Coefficient Method

When natural periods of structures are close to dominant periods of earthquake ground motion, dynamic response of those structures is amplified. However, the inertia force by the seismic coefficient method is always constant without any relationship to the amplification of response acceleration.

A modified seismic coefficient method is proposed to solve this limitation. Seismic intensity coefficient is required to change with the natural period of structures. Figure 2.4 depicts the K_H in *Specifications for Highway Bridges and*

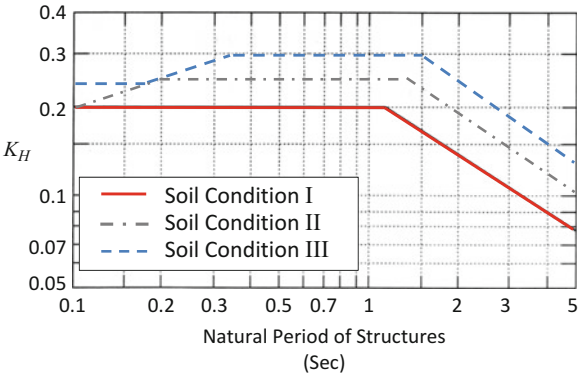

Fig. 2.4 Seismic coefficients K_H for modified seismic coefficient method (Specification for Highway Bridges and Explanation, Part *V*, Seismic Design [3])

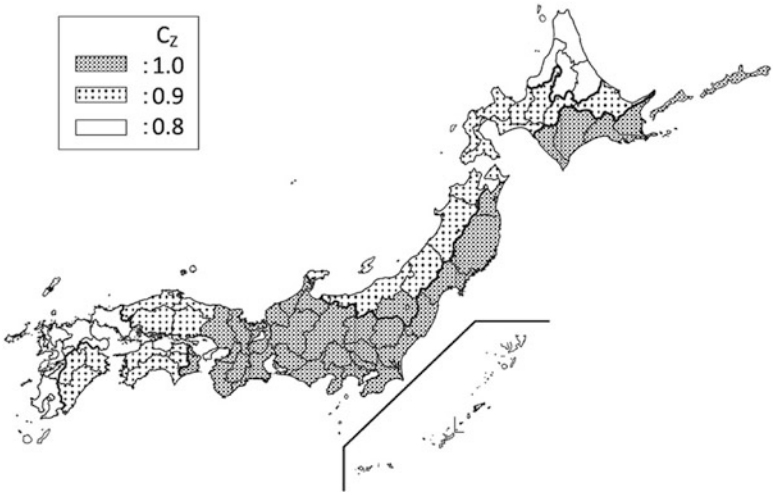

Fig. 2.5 Regional coefficients for modification of seismic coefficient (Specification for Road Bridges and Explanation, *V* earthquake resistant design [3])

Explanation Part V, Seismic Design [3]. The horizontal axis indicates the natural period of structures, and K_H is determined by natural periods of structures and soil condition (I to III). The horizontal force H on the structures can be obtained from

$$H = C_Z \cdot K_H \cdot W \tag{2.6}$$

where C_z is the regional coefficient; values of 0.8–1.0 were adopted (Fig. 2.5) according to regional seismic activities. Figure 2.4 indicates that K_H is relatively large for periods between 0.3 s and 1.5 s under the soil condition III. This follows from the fact that earthquake ground motions are generally dominant in these periods.

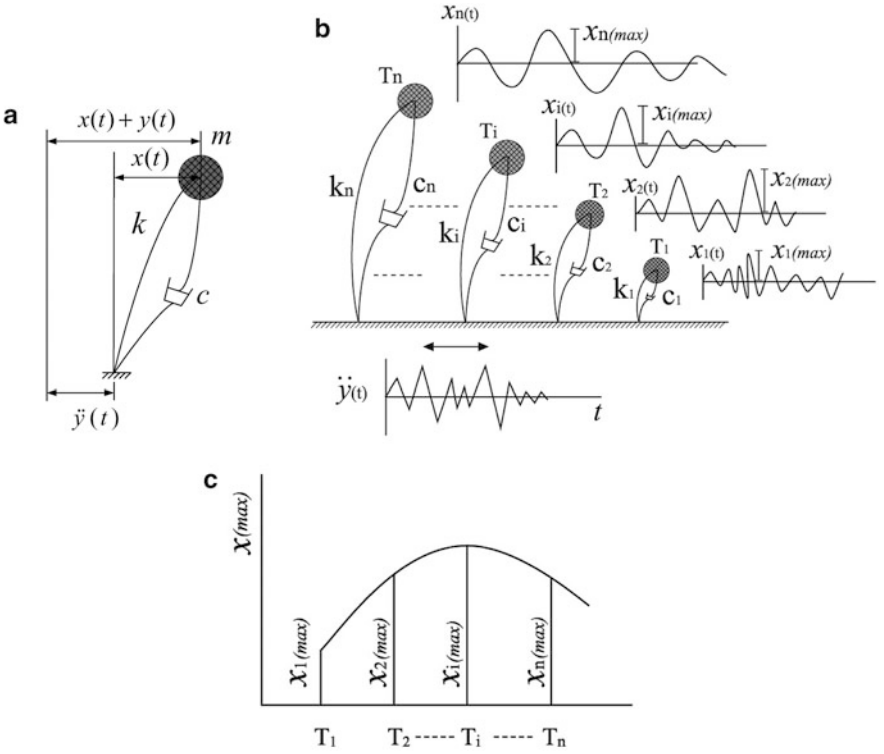

Fig. 2.6 Calculation of response spectra. (**a**) Dynamic response of single mass-spring-damper model. (**b**) Maximum displacements response of each mass-spring-damper model. (**c**) Displacement response spectra

Soil conditions I to III are determined based on the natural period of the surface ground. Type III represents soft soil such as alluvial plain and reclaimed land, whereas type I indicates hard soil such as diluvial ground and bedrock. Type II specifies soil intermediate to types I and III. Figure 2.4 is termed a response spectrum, and is calculated by the method described below.

2.1.4 Response Spectra

As displayed in Fig. 2.6a, the vibration equation of one-mass-spring-damper model can be expressed as

$$\ddot{x}(t) + 2\omega_0 h\dot{x}(t) + \omega_c^2 x(t) = -\ddot{y}(t) \tag{2.7}$$

where $x(t)$ is displacement of one mass (relative displacement from the fixed point of the spring). $\dot{x}(t)$ and $\ddot{x}(t)$ are velocity and acceleration of the mass, respectively.

ω_0 is the circular natural frequency of the one-mass-spring-damper model and h is the critical damping constant. They can be written as follows:

$$\omega_0 = \sqrt{\frac{m}{k}}$$
$$h = \frac{c}{2\omega_0 m} \tag{2.8}$$

where m and k are the mass and spring constants, respectively, and c is the viscous damping coefficient.

The solution of Eq. (2.7), relative displacement $x(t)$ relative velocity $\dot{x}(t)$, and absolute acceleration $\ddot{x}(t) + \ddot{y}(t)$ of the one-mass-spring-damper model can be obtained as follows:

$$x(t) = -\frac{1}{\omega_0\sqrt{1-h^2}}\int_0^t \exp[-\omega_0 h(t-\tau)] \cdot \sin\omega_0\sqrt{1-h^2}(t-\tau)\cdot\ddot{y}(\tau)d\tau \tag{2.9}$$

$$\dot{x}(t) = -\int_0^t \exp[-\omega_0 h(t-\tau)]\cdot \left\{\cos\omega_0\sqrt{1-h^2}(t-\tau) - \frac{h}{\sqrt{1-h^2}}\sin\omega_0\sqrt{1-h^2}(t-\tau)\right\}\ddot{y}(\tau)d\tau \tag{2.10}$$

$$\ddot{x}(t) + \ddot{y}(t) = \omega_0\frac{1-2h^2}{\sqrt{1-h^2}}\int_0^t \exp[-\omega_0 h(t-\tau)] \cdot \sin\omega_0\sqrt{1-h^2}(t-\tau)\cdot\ddot{y}(\tau)d\tau + 2\omega_0 h\int_0^t \exp[-\omega_0 h(t-\tau)]\cos\omega_0\sqrt{1-h^2}(t-\tau)\cdot\ddot{y}(\tau)d\tau + \ddot{y}(t) \tag{2.11}$$

By taking the maximum value irrespective of time t of the relative displacement, relative velocity and absolute acceleration, the response spectra S_D, S_V, and S_a are as follows:

$$S_D = |x(t)|_{\max} \tag{2.12}$$

$$S_V = |\dot{x}(t)|_{\max} \tag{2.13}$$

$$S_A = |\ddot{x}(t) + \ddot{y}(t)|_{\max} \tag{2.14}$$

Generally, h is much smaller than 1.0 for ordinary structures, hence, the response spectra S_D and S_V can be rewritten as

$$S_D = \frac{1}{\omega_0}\left|\int_0^t e^{-\omega_0 h(t-\tau)} \cdot \sin\omega_0(t-\tau)\cdot\ddot{y}(\tau)d\tau\right|_{\max} \tag{2.15}$$

$$S_V = \left| \int_0^t e^{-\omega_0 h(t-\tau)} \cos \omega_0 (t-\tau) \cdot \ddot{y}(\tau) d\tau \right|_{\max} \tag{2.16}$$

The input acceleration $\ddot{y}(t)$ in Eq. (2.11) can be neglected, because its influence on the maximum value of the absolute acceleration $\ddot{x}(t) + \ddot{y}(t)$ is limited. The following can be obtained:

$$S_A = \omega_0 \left| \int_0^t e^{-\omega_0 h(t-\tau)} \cdot \sin \omega_0 (t-\tau) \cdot \ddot{y}(\tau) d\tau \right|_{\max} \tag{2.17}$$

If the earthquake ground motion $y(\tau)$ in Eqs. (2.15), (2.16) and (2.17) are sufficiently long, the influence of the difference obtained by multiplying it by either sin $\omega_0(t - \tau)$ or cos $\omega_0(t - \tau)$ becomes negligible, and the following equations are obtained:

$$S_D \fallingdotseq \frac{1}{\omega_0} \cdot S_V \tag{2.18}$$

$$S_A \fallingdotseq \omega_0 \cdot S_V \tag{2.19}$$

That is, all the response spectra can be defined if the displacement, velocity, or acceleration spectrum is obtained. When the time history of the input acceleration $\ddot{y}(t)$ is given, the maximum displacement $|x(t)|_{\max}$ of each one-mass-spring-damper model with different natural circular frequency ω_0 (natural period $T = 2\pi/\omega_0$) under a constant critical damping constant h, can be obtained as shown in Fig. 2.6b. Figure 2.6c is the displacement response spectrum where the values of the maximum displacement of each mass-spring-damper model are plotted with the natural periods of the models $T_1 \sim T_n$ in the horizontal axis. Generally, the response spectra is given at $h = 0.05$ (5 %) for ordinary structures. For sloshing vibration of the contents of large storage tanks (referred to Sect. 2.2.3), $h \fallingdotseq 0.5$ % is usually used. This is because damping of the sloshing vibration, e.g., that of crude oil in large tanks, is very small.

As a method for analyzing dominant periods in an earthquake ground motion of random time history, the Fourier spectrum is generally used. However, the aforementioned response spectrum can also depict dominant components of earthquake ground motions. The response spectra have more engineering-oriented information.

Figure 2.7a shows an example of horizontal accelerations at the ground surface and their response spectra at K-NET [2] in Sendai during the 2011 Tohoku earthquake. The maximum accelerations were 1,517 and 982 cm/s^2 in the north–south and east–west directions, respectively. The response acceleration in the north–south direction exceeded 2,000 cm/s^2 between 0.5 and 0.8 s as shown in Fig. 2.7b. This demonstrates that the earthquake ground motion was dominant in these periods, and that dynamic responses of structures with these natural periods are amplified.

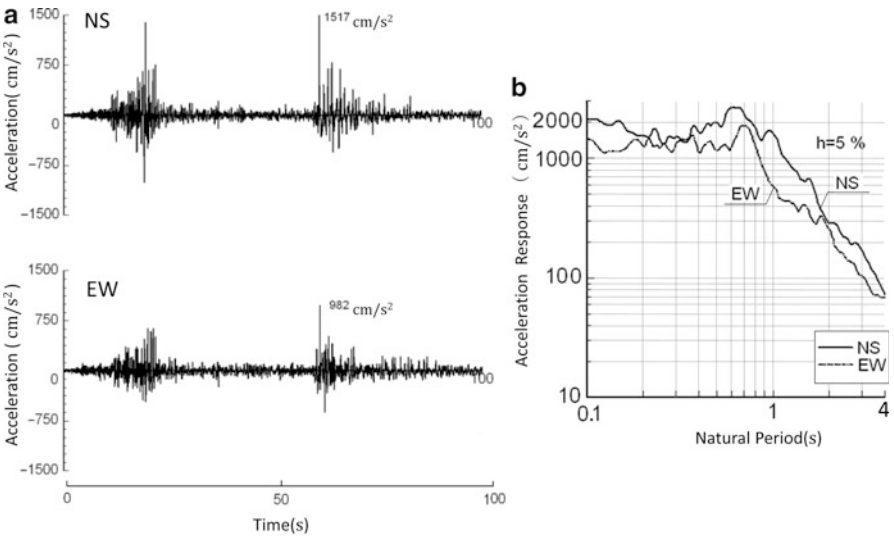

Fig. 2.7 Ground acceleration and acceleration response spectra (2011 Tohoku earthquake at Sendai K-NET). (**a**) Accelerations observed at the ground surface. (**b**) Acceleration response spectra

2.2 Development of Earthquake-Resistant Design

The seismic coefficient method was proposed in 1917, followed by a modified seismic coefficient method. The latter method, in which the seismic coefficient is changed according to natural periods of structures, has been widely used in earthquake-resistant design. However, earthquake-resistant design methods have been repeatedly revised, based on knowledge and experience from past earthquake damage.

2.2.1 Earthquake-Resistant Design Against Soil Liquefaction

In the 1964 Niigata earthquake, liquefaction of sandy ground was firstly recognized from an engineering perspective. Sand and ground water boils were observed within wide areas along the Shinano and Agano rivers in Niigata, and many structures subsided and inclined. Figure 2.8a shows a three-story reinforced concrete building steeply inclined by soil liquefaction. The building was constructed on a mat foundation. As addressed in Sect. 4.1.3, girders of the Showa Bridge fell into the river because of large ground displacement caused by the flow of liquefied soil (Fig. 4.19). Many underground structures such as purification tanks and sewage manholes were lifted by the buoyancy of liquefied soil (Fig. 2.8b).

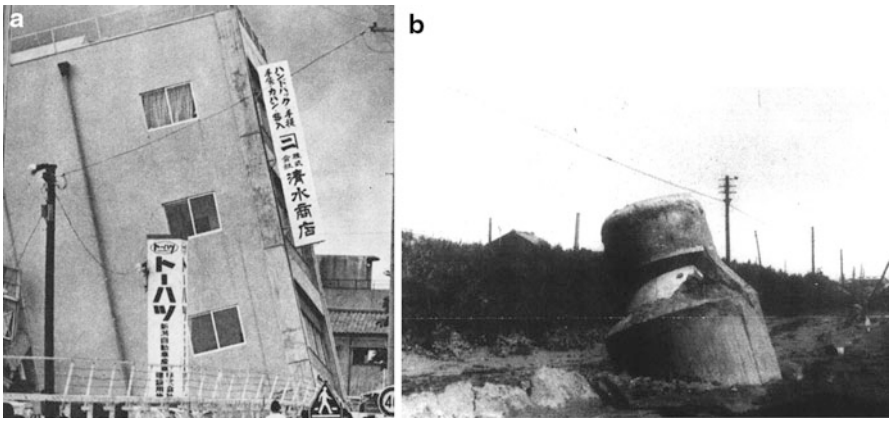

Fig. 2.8 Liquefaction-caused damage (1964 Niigata earthquake). (**a**) Inclination and subsidence of a three-story RC building. (**b**) Uplift of sewage manhole

At the time it was difficult for scientists and engineers to satisfactorily explain the mechanism of soil liquefaction and its damage to structures. They thought that a kind of "quick sand phenomenon", in which sand loses strength because of vibration, occured. However, a report on the Niigata earthquake by the Japan Society of Civil Engineers (JSCE) [4] called the phenomenon over the entire region of Niigata as "sand flow" or "ground flow." From this description, it can be imagined that a large amount of sand moved horizontally.

From the 1964 Niigata earthquake and subsequent earthquakes, the following have been explained as damage from soil liquefaction:

(i) Inclination and subsidence by loss of bearing capacity of the ground
(ii) Uplift of underground structures by buoyancy of liquefied soil
(iii) Collapse of earth structures such as embankments and levees by loss of strength of soil
(iv) Collapse and inclination of quay walls and retaining walls by increase of earth pressure

With these types of liquefaction-induced damage as motivation, methods for estimation of liquefaction potential and various countermeasures against soil liquefaction were developed for practical use.

After the 1983 Central Japan Sea earthquake, ground displacements caused by the flow of liquefied soil were first measured. In addition, ground displacement caused by the 1964 Niigata earthquake was measured anew. Furthermore, the relationship between damage to foundation piles and buried pipes, and measured ground displacements was investigated. Japan–U.S. cooperative research was done to clarify the mechanism of large ground displacements by liquefied soil flow, and

to develop countermeasures against such displacements. Despite these efforts, liquefaction-induced large ground displacements were again caused in reclaimed lands during the 1995 Kobe earthquake, inflicting damage to bridges, buildings and lifeline facilities.

With consideration of such damage, studies for earthquake-resistant designs and countermeasures against liquefaction-induced large ground displacements were promoted. Descriptions of countermeasures and estimation of ground displacement are provided in Chaps. 3 and 4, respectively.

2.2.2 *Lifeline Earthquake Engineering*

"Lifeline" was originally a maritime word meaning "life-saving rope" or "life preserver." In the context of protecting human life by constructing the environment for daily life in populated cities, the word is used as a comprehensive expression of systems for maintaining city function. In an earthquake engineering conference in the United States in 1975, "Lifeline Earthquake Engineering" was proposed. With this as motivation, water, sewage, electric power, gas, telecommunication, and others came to be called lifeline systems [5].

Lifeline systems are generally classified based on the services they supply:

(1) Water supply and purification systems—water, sewage, and river facilities (intake and discharge of water)
(2) Energy systems—electric power, city gas, and local cooling/warming
(3) Information and communication systems—telephone, information and broadcast facilities
(4) Transportation systems—roads, railroads, ports, airports

In the 1978 Miyagi offshore earthquake, there was serious damage to buried pipes of lifeline systems, such as water, sewage and gas in residential areas in the hills of suburban Sendai. The main cause of damage to those pipes was differential vertical ground displacements between zones reclaimed from valleys and those developed by excavation of ridges. After the earthquake, research for strengthening earthquake resistance of buried pipes was promoted. In 1982, *Standard for Earthquake Resistant Design of High Pressure Gas* [6] was compiled by the Japan Gas Association. In this standard, methods for earthquake-resistant design of buried pipes against ground surface fissures and differential settlement of ground were taken into the consideration.

The 1985 Kobe earthquake inflicted unprecedented damage to urban lifeline systems in the Kobe and Osaka districts. The summary of the damage to various lifeline systems, and recovery days are shown in Table 1.3 of Sect. 1.3. Details of damage to water and sewage systems and recovery days are shown in Tables 2.1 and 2.2.

Table 2.1 Damage to water systems by the 1955 Kobe earthquake and days for recovery

City	Number of households in suspension of supply (rate)	Direct money loss (Yen)	Days for recovery	Mainly damaged facilities
Kobe	650,000 (100 %)	31,570,000	70	Purification plants Transmission pipes Distribution pipes Buildings
Nishinomiya	157,000 (95 %)	4,580,000	70	Reservoir Transmission pipes Distribution Pipes
Amagasaki	193,000 (100 %)	308,000	14	Transmission pipes Distribution pipes
Ashiya	33,400	1,474,000	64	Purification plants Tunnels
Hyogo prefecture	1,265,730	55,759,000		

Table 2.2 Damage to sewage systems by the 1955 Kobe earthquake and days for recovery

City	Total length of pipes (m)	Damaged length (m) (rate)	Direct economic loss (Yen)	Mainly damaged facilities and days for recovery
Kobe	3,315,392	73,005 (2.2 %)	51,425,972	Waste water treatment plants and pumping stations by strong ground motion and soil liquefaction
Amagasaki	1,019,290	45,583 (4.4 %)	1,562,431	Days for recovery Pipes: 140 days (Kobe) Waste water treatment plants: 5 months
Nishinomiya	916,900	32,088 (3.4%)	11,963,615	
Ashiya	215,400	28,548 (13.3 %)	6,155,764	
Takarazuka	531,800	8,597 (1.6 %)	1,504,239	
Hyogo prefecture	7,491,982	198,510 (2.6 %)	73,456,585	

For water supply to Kobe, Nishinomiya and Ashiya cities, it took about 70 days to recover from damage to purification plants, distribution and transmission pipes, and others. Most notably, the city water works office in Kobe, on the 5th floor of the city hall, collapsed by the earthquake (Fig. 1.61a). Thus, documents regarding facilities and buried pipes were unusable, greatly hindering restoration work.

The water conveyance tunnel in Ashiya (Fig. 1.61f) was damaged. This may be attributed to strong earthquake ground motion near the active fault and shallow depth of the tunnel.

Major causes of damage to sewage facilities are strong earthquake ground motion and soil liquefaction. Liquefaction at the Higashinada wastewater treatment plant was particularly severe. The ground moved toward the canal about 3 m, and foundation piles of the administration building and sewage treatment plants were ruptured and the buildings inclined. This caused the recovery to take about 5 months. Details of the damage to the waste water treatment plant will be given in Sect. 4.1.4.

Causes of damage to the lifeline systems were as follows:

(i) Extensive soil liquefaction and large ground displacement by liquefied soil flow in the reclaimed land damaged key stations, such as wastewater treatment plants, purification plants, and buried pipes.
(ii) There were large numbers of decayed and old pipes of low strength.
(iii) Earthquake ground motion far exceeded the design level.

Reasons for the very long recovery time were as follows:

(i) The database of buried pipes was inadequate, and it took much time to detect pipe damage.
(ii) Transportation of equipment/personnel was hindered due to traffic congestion.
(iii) Recovery work was entangled with that on other lifeline systems.

After the 1995 Kobe earthquake, there were comprehensive revisions of earthquake-resistant design codes for water, sewage, city gas, electricity, and telecommunication. In these revisions, earthquake ground motion for the design was greatly increased. Concurrently, the effect of liquefaction-induced large ground displacement came to be considered. Furthermore, support systems for restoration of lifelines among municipalities were nationwide established.

In the 2004 Niigata-Chuetsu offshore earthquake, more than 1,400 sewage manholes were lifted in Nagaoka, Ojiya and other cities. This was mainly attributed to the liquefaction of backfilling soil around the manholes. Therefore, various countermeasures have been developed and applied, namely, compaction of backfilling soil, gravel and rock filling, and hardening of soil by cement milk. Furthermore, several countermeasures against soil liquefaction of existing manholes were developed. Details are described in Sect. 3.3.3.

Numerous waste water treatment plants and pumping stations were severely damaged by the tsunami of the 2011 Tohoku earthquake. Because of loss of power sources by tsunami inundation, inflow of floating objects to the sedimentation basins, and flowing-out of machineries, sewage treatment functions were stopped for a long period. For this reason, the *Fundamental Concept for Promoting Anti-Tsunami Measures* was established by the "Committee for Anti-Earthquake and Tsunami Measure of Sewage System". Details are described in Sect. 2.8. Furthermore, there were another kinds of sewage pipelines damage such as horizontal differential displacement of concrete ring elements of manholes, pullout of sewage pipes connecting manholes, and inflow of liquefied soil. An example of liquefied soil flow into a manhole is shown in Fig. 2.9.

Fig. 2.9 Liquefied soil flow into a manhole (2011 Tohoku earthquake)

2.2.3 Earthquake-Resistant Design Against Long-Period Ground Motion

The 2003 Tokachi offshore earthquake caused fires of crude oil and naphtha tanks of an oil refinery in Tomakomai (Fig. 1.67). Long-period earthquake ground motion triggered sloshing vibration of the contents of floating roof-type tanks. It is also assumed that fire broke out from collision of metal fragments of the tanks. Tank fires by long-period component of earthquake motions have been caused in earthquakes greater than mid–scale, such as the 1964 Niigata and 1999 Kocaeli (Turkey) earthquakes. A large number of floating-roof type tanks have been constructed in oil and chemical industrial complexes in Japan. Around Tokyo Bay, the number of such tanks exceeds 600. Several methods to suppress the sloshing vibration of tank contents have been proposed, but none have been practically used to control vibration of content in tanks with diameters of several tens of meters. Moreover, for tanks that have already been constructed, it is difficult to install devices to suppress the sloshing vibration.

Given such difficulty, the following countermeasures are taken for preventing fires from the sloshing in the floating roof-type tanks:

(i) Reinforcement of floating roofs by double deck structures
(ii) Reinforcement of barrier walls for outflow of oil against soil liquefaction
(iii) Installation of equipments and preparations for rapid firefighting

After the 2003 Tokachi offshore earthquake, design codes for oil tanks, petrochemical products, and high-pressure gas were updated. The height of liquid rise W_h induced long-period ground motion can be expressed as follows [7]:

$$W_h = \frac{R}{g} \cdot 0.837 \left(\frac{2\pi}{T_S} \right) \cdot S_V \tag{2.20}$$

Here, R indicates the radius of the tank (in m), and g is the acceleration of graviation (9.8 m/s^2). T_S is the first natural period of the sloshing vibration of tank contents, which is

$$T_s = 2\pi\sqrt{\left(\frac{R}{1.84g}\right)\coth\left(3.68\frac{H}{D}\right)} \tag{2.21}$$

Here, H is depth of the contents (in m).

S_V (m/s) is the velocity response spectrum from long-period ground motion, which is

$$S_V = S_{V0} \cdot \nu_5 \tag{2.22}$$

S_{V0} is the standard velocity response spectrum, and is shown in Fig. 2.10a for four areas in Japan. ν_5 is a coefficient reflecting the likelihood of long-period earthquake ground motion, which is shown for several areas with major oil refinery complexes in Fig. 2.10b. The response spectra were attained by observation of long-period earthquake ground motions and by a survey of deep soil conditions.

The volume of overflowing liquid ΔV of tank contents can be obtained from

$$\Delta V = \pi R^2 \cdot \frac{\alpha \cdot \delta_h (R - r_0)\theta_0}{R} \tag{2.23}$$

δ_h (in m) in this equation is the height of overflow (Fig. 2.11) [7]. This can be determined from the difference between the height of liquid rise W_h and the original depth of content surface from the top of the sidewall H_c (in m). θ_0 is an angle allowing the sloshing wave height to equal H_c. r_0 denotes the horizontal distance from the tank center to the intersection of the sloshed oil surface with the horizontal plane at the level of the sidewall top. α is a coefficient expressing the control effect on the sloshing vibration of the floating roof, and is generally taken as 0.4023.

2.3 Performance-Based Earthquake-Resistant Design Against Two Levels of Earthquake Ground Motion

2.3.1 JSCE Recommendation for Earthquake-Resistant Design and Reinforcement of Existing Structures

The 1995 Kobe earthquake killed more than 6,000 people and destroyed various types of infrastructures such as roads, railways, ports and lifelines. The response acceleration of earthquake ground motion in Kobe (Fig. 1.60) reached approximately 2,000 cm/s^2 in the period range from 0.3 to 1.0 s. The acceleration greatly

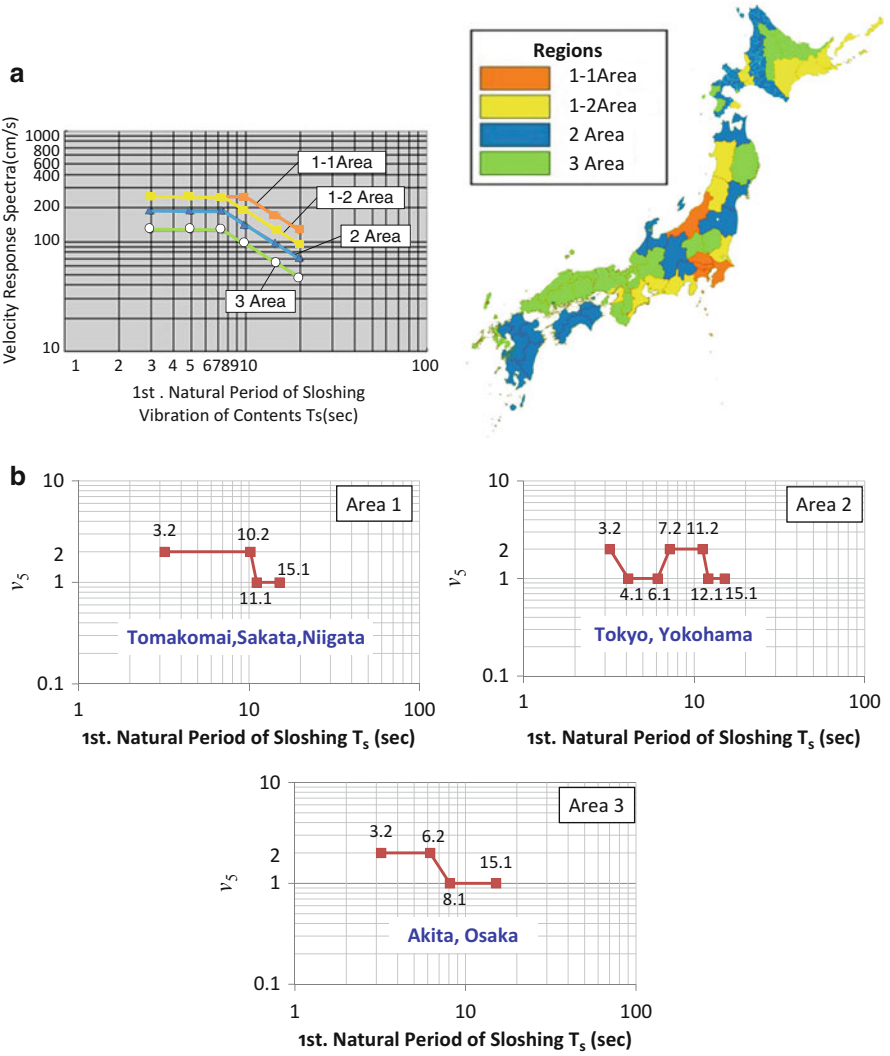

Fig. 2.10 Velocity response spectra for estimation of sloshing wave height of tank content (S_{v0}) [8]. (**a**) Velocity response spectra (critical damping constant h = 0.5 %). (**b**) Regional coefficients based on likelihood of occurrence of long period ground motion

exceeded the 1,000 cm/s^2 that had been used for earthquake-resistant design of road bridges and railway facilities prior to the earthquake, in which plastic deformation of structures was considered.

In response to the severe damage to numerous structures from the Kobe earthquake, the JSCE "Ad Hoc Committee of Basic Principles for Earthquake-Resistant Design and Reinforcement of Existing Structures" recommended the

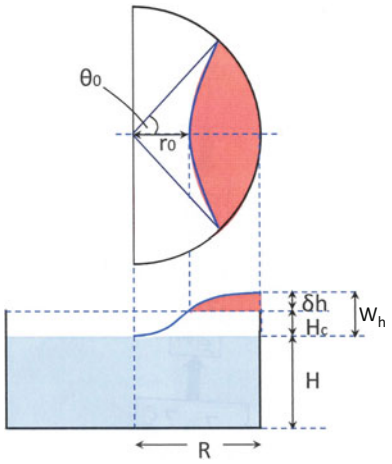

$$\Delta V = \pi R^2 \cdot \frac{\alpha \cdot \delta_h (R - r_0)\theta_0}{R}$$

ΔV : Total Volume of Overflow
R : Radius of Tank
α : Control Coefficient(Floating Roof Tank : 0.4023)
δ_h : Height of Overflow
H_C : Depth of Content Surface from Top of Side Wall
r_0 : Horizontal Distance between Tank Center and The Intersection of Sloshed Oil Surface with Horizontal Plane
θ_0 : Angle Allowing Sloshing Wave Height to Equal H_C
W_h : Wave height of Sloshing

Fig. 2.11 Sloshing vibration of contents of circular tanks by long period ground motion [8]

following fundamental policies for earthquake-resistant design and reinforcement of existing structures [8].

(i) Two levels of earthquake ground motions should be considered in earthquake-resistant design. Level 1 earthquake ground motion has a probability of occurrence of once or twice during structure's lifetime. Level 2 earthquake ground motion has low probability of occurrence, but strong shaking such as observed around Kobe during the 1995 earthquake.
(ii) Structures should be designed to satisfy requisite performances during and after the earthquakes assumed in the design. Those performances are determined by considering the probabilities of occurrence of level 1 and 2 earthquake ground motions, plus effects on human lives, rescue operations, restoration and reconstruction works. The most important point for earthquake resistant design of structures from requisite performance against level 2 earthquake ground motion is to prevent structures from total collapses for saving human lives. This design method is called performance-based design. This concept is applied for the earthquake-resistant design of all civil engineering structures, including earth structures such as embankments, river levees and dams.

The recommendation by JSCE is based on the most important lesson learned from the 1995 Kobe earthquake. That is to save lives, even when structures encounter strong ground motion as in the Kobe earthquake. The JSCE recommendation was incorporated in one of the national policies on earthquake-resistance of structures. In the *Basic Plan for Disaster Prevention* published by the Cabinet Office, Government of Japan, the following were declared in Chap. 1 ("Creation of Safe Nation and Community against Future Earthquakes") [9].

(i) Two types of earthquake ground motions should be considered for the design of structures. The first is motion with a probability of occurrence once or twice during the structure lifetime. The second is strong motion caused by inland earthquakes or huge earthquakes along sea troughs, which have comparatively low probabilities of occurrence.
(ii) Structures shall be designed with the fundamental objective that human lives not be lost to strong earthquake ground motion, and that post-earthquake rescue operations and regional economic activities not be seriously affected.

Given the concept of earthquake resistance of structures in the *Basic Plan for Disaster Prevention* as fundamental policy for their earthquake-resistant design after the Kobe earthquake, the following standards and codes were revised.

- *Specifications for Highway Bridges, and Explanation Part V Seismic Desig*n *(1996)* , Japan Road Association [3]
- *Guidelines for Earthquake-resistant Measures for Sewage Facilities and Explanation (1997)*, Japan Sewage Works Association
- *Basic Principles of Seismic Design and Construction for Water Supply Facilitie*s (1997), Japan Water Works Association [10]
- *Guidelines for Earthquake-resistant Design of High Pressure Gas Facilities (1997)*, The High Pressure Gas Safety Institute of Japan
- *Seismic Design for Railway Structures and Commentary (1999)*, Railway Technical Research Institute [11]
- *Technical Standards and Commentaries for Port and Harbor Facilities (1999)*, Bureau of The Ports of Harbor, Ministry of Transport [12]
- *Guidelines for Earthquake-resistant Design of High Pressure Gas (2000)*, The Japan Gas Association
- *Guidelines for Earthquake-resistant Design of Gas Facilities (2001)*, The Japan Gas Association
- *Guidelines for Earthquake-resistant Design of High Pressure Gas Facilities against Liquefaction (2001)*, The Japan Gas Association

The concept of performance based design against two levels of ground motion is illustrated in Fig. 2.12 [12]. Figure 2.12a shows an example of relationship between seismic force and displacement at the top of a concrete bridge pier. As seismic force increases, cracks appear in the concrete, and further increase of the force results in yielding of reinforced steel bars. After that, the pier collapses via maximum load. Design should not allow residual deformation during level 1 earthquake ground motion, although cracks in the concrete will remain after the earthquake. In this case, nearly the same earthquake resistance should be guaranteed after the earthquake, without any repair. For level 2 earthquake ground motion, the design is aimed at recovery of function and prevention of collapse. Function of the pier should be recovered, for an example, in 2 or 3 weeks, even with damage to the upper structure and foundation. Assessment of the earthquake-resistant performance of the piers (Fig. 2.12c) is made based upon the extent of damage to superstructures and the foundation, along with the residual displacement.

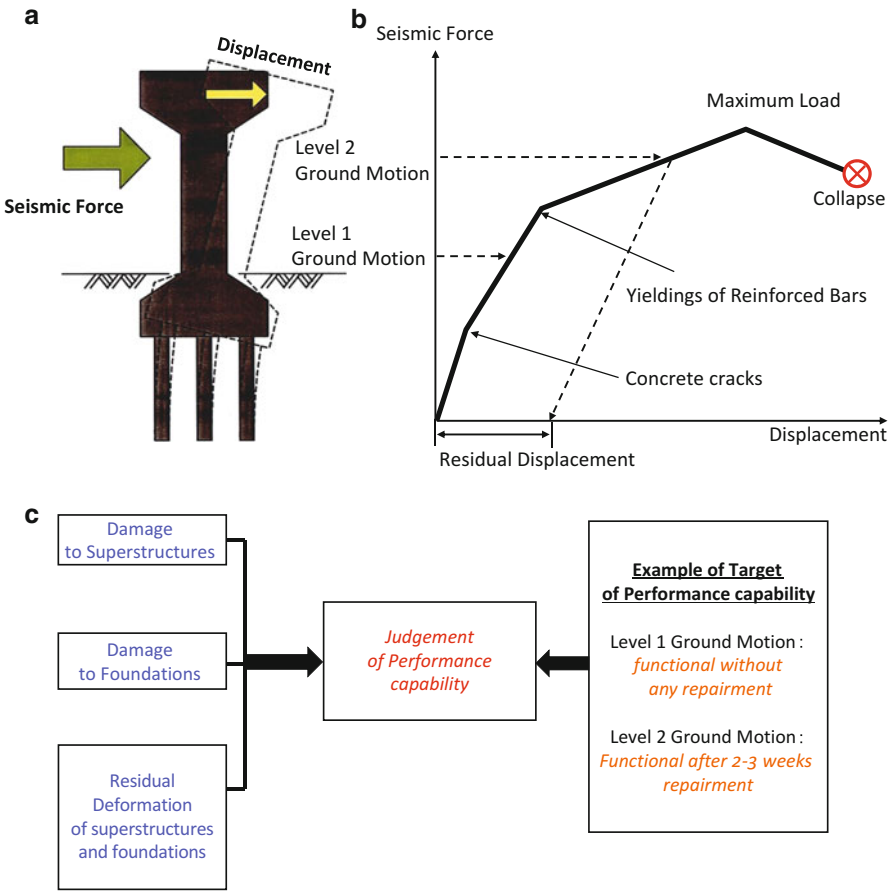

Fig. 2.12 Performance-based design against two-levels of earthquake ground motion. (**a**) Seismic force on reinforced concrete Pier and displacement. (**b**) Relationship between seismic force and displacement. (**c**) Judgment of performance capability

2.3.2 Setting of the Two Levels of Ground Motion

For performance-based design against the two levels of earthquake ground motion, it is necessary to determine those levels. The ground motion used in earthquake-resistant design before the 1995 Kobe earthquake is adopted, as level 1 ground motion in most of the design codes.

For level 2 motion, two methods are available. The first is to directly deduce earthquake ground motion by investigating active faults near the construction site of structures that will affect their seismic safety. In this case, the ground motion is calculated by numerical analyses based on the fault failure process and seismic wave propagation toward the site. In the second method, a standard ground motion

is determined based on ground motions observed during past earthquakes. The design ground motions are attained by modification of the standard ground motion, depending on the seismic activity in the region.

In the first method, it is sometimes difficult to avoid overlooking active faults. Furthermore, various parameters governing the failure process of faults are required for calculating earthquake ground motion, but it is not easy to determine these parameters from fault surveys.

In most cases of the second method, the maximum ground motion observed during past earthquakes is used as the design motion. However, that maximum ground motion is occasionally exceeded in subsequent earthquakes. Every time a new higher ground motion is recorded, the design ground motion should be revised. In the 2004 Niigata-Chuetsu offshore earthquake and 2008 Iwate-Miyagi inland earthquake, maximum accelerations greatly exceeded that in the 1995 Kobe earthquake (Figs. 1.71 and 1.89). For this reason, a new concept of exceedence probability was introduced for earthquake-resistant design of buried water and sewage pipes and facilities of key stations, such as water purification plant and waste water treatment plant.

In the design codes revised after the Kobe earthquake, two types of earthquakes were considered to induce level 2 ground motion. Type 1 are earthquakes near the plate boundary in the Pacific Ocean with magnitude of 8 or more. These earthquakes have been already considered in the design of highway bridges and railway facilities before the Kobe event. Type 2 are earthquakes caused by inland faults with magnitude in the 7 class, which was not considered before the Kobe earthquake.

In the "*Specification for Highway Bridges and Explanation, Part V, Seismic Design*," revised in 1996, response spectra were shown for each type (1 and 2) of earthquake, as shown in Fig. 2.13 [3]. In these figures, soil conditions I and III refer to hard and soft soil, respectively, as mentioned in Sect. 2.1.3. In type 1 earthquakes, spectra for ground condition III are higher than that for soil condition I. However, in type 2 earthquakes, spectra for soil condition I are higher than for soil condition III. This is because non-linearity of soft soil increases against the strong earthquake ground motion near inland faults, and decrease of the response at the ground surface is considered.

In the standards of railway structures [11], a flowchart as shown in Fig. 2.14 is recommended for determination of level 2 ground motion. In this flowchart, whether inland active faults existence is firstly investigated. Second, if it is determined that such faults do not exist, the standard spectrum I by plate-boundary earthquakes is used, with adjustment for epicentral distance. If it is ascertained that inland active faults exist and determination of the parameters of fault failure is possible, design ground motion is directly determined by numerical analysis(Spectrum III). When identification of those parameters is impossible, standard spectrum II, which is made based on ground motions observed during past earthquakes caused by inland faults, is adjusted by the regional seismic activity. When the existence and locations of inland faults are unknown, the standard spectrum II is adjusted by the regional seismic activity.

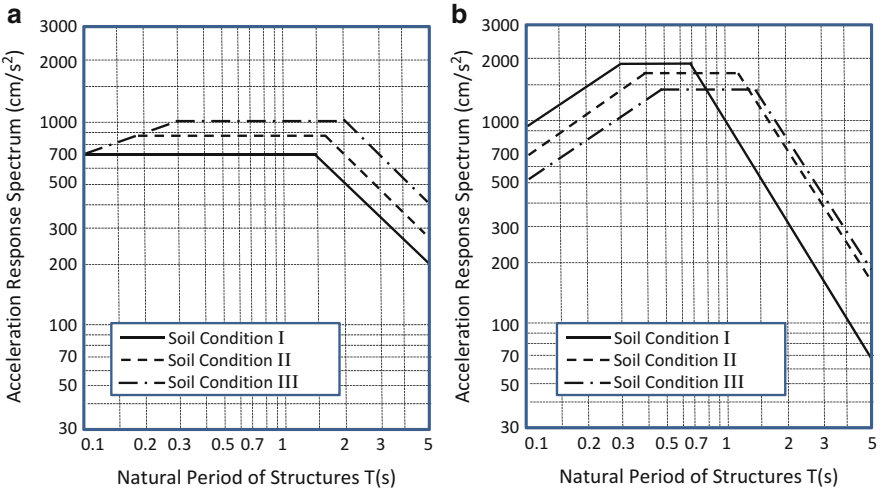

Fig. 2.13 Design spectra of level 2 earthquake ground motions for design of road bridges [3]. (**a**) Acceleration response spectra of type 1 earthquake ground motion. (**b**) Acceleration response spectra of type 2 earthquake ground motion

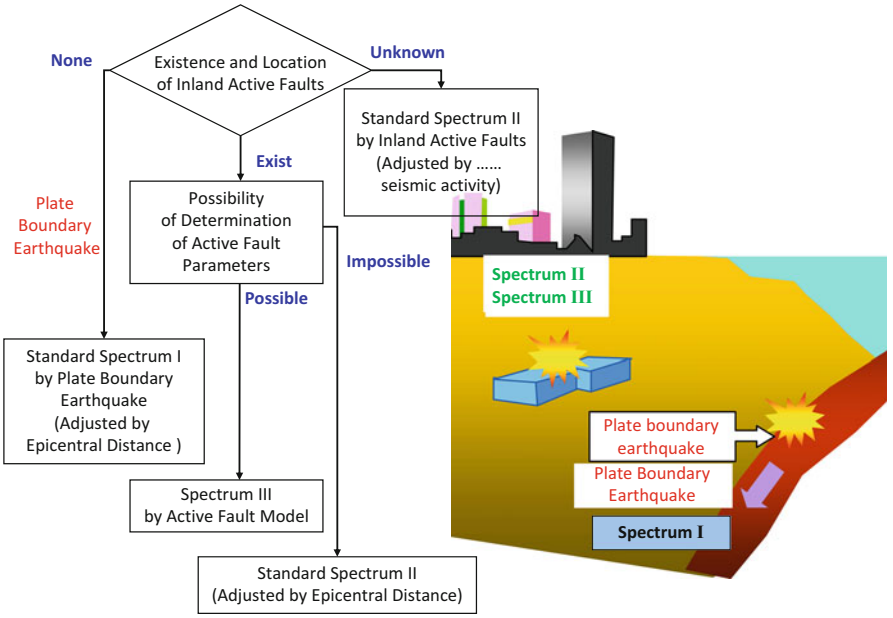

Fig. 2.14 Flow of setting of level-2 earthquake ground motion for railway structures [12]

2.4 Dynamic Response of Ground

2.4.1 Amplification of Earthquake Motion at Ground Surface and Dominant Periods

Figure 2.15 shows horizontal accelerations observed in reclaimed land around Tokyo Bay during the 2011 Tohoku earthquake and their Fourier spectra. As depicted in Fig. 2.15a, the ground at the observation point is composed of filled soil to −13 m elevation and alternating layers of sand and clay including gravel to −42 m. Layers deeper than −42 m are hard gravel or sand layers with N values exceeding 50, which can be regarded as bedrock. S-wave velocities of the ground above the bedrock are 160–240 m/s. Earthquake ground motion was observed at the ground surface and at depths −22 and −53 m from the ground surface in the hard gravel layer. Figure 2.15b shows that acceleration at the ground surface was much greater than those in the ground, and it is understood that the earthquake motion was amplified. Fourier spectra of the acceleration in Fig. 2.15c show that the earthquake motion was amplified in the frequency domain from 0.8 to 1.6 Hz. Amplification of the earthquake motion at 1.2 (1/s) was especially significant; this frequency is recognized as the natural period of the surface ground. The above findings reveal that earthquake motion at the ground surface had two characteristics: (i) amplification, and (ii) dominant vibration at specific frequencies.

2.4.2 Seismic Waves and Propagation

Seismic waves consist of body waves, which are P (primary) and S (Secondary) waves, and surface waves, which are Rayleigh and Love waves (Fig. 2.16). P and S-waves directly propagate in the earth crust and soil from the fault to the ground surface. The Rayleigh and Love waves, which are generated after the body (P and S) waves reach the surface, propagate along the surface.

Vibration by S-wave is a major constituent of earthquake ground motion, and oscillates structures such as bridges, dams, low- and medium-rise buildings. This is because the dominant periods of an S-wave are mostly shorter than 1 s, and coincide with natural periods of these structures.

The Rayleigh and Love waves generally have a long-period vibration component of several seconds. This component of vibration is amplified by the deep structure of ground, and induces sloshing vibration of oil in large tanks. These waves also affect earthquake resistance of high-rise buildings and long-span bridges. An example of tank fires from sloshing vibration caused by long-period components of earthquake ground motion is given in Section 1.3.4. The earthquake-resistant design of tanks against long-period ground motion was treated in Sect. 2.2.3.

Consider an S-wave propagating through homogeneous surface ground in a vertical direction (Fig. 2.17a). The wave equation of S-wave propagation can be obtained by considering the equilibrium of forces on soil segments at depth $z = z$.

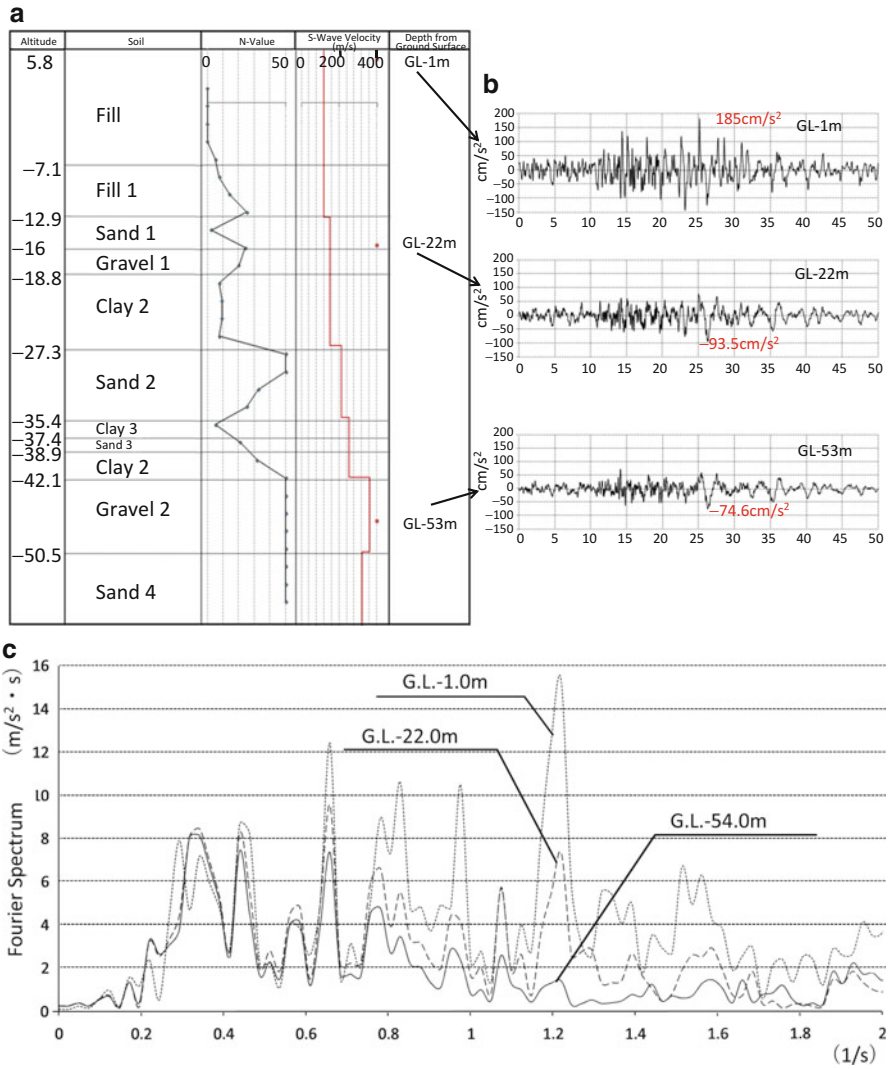

Fig. 2.15 Earthquake ground motion observed in artificial land reclaimed from the Tokyo Bay (2011 Tohoku earthquake). (**a**) Soil condition. (**b**) Observed ground motion. (**c**) Fourier spectra of observed ground acceleration

The equilibrium equation can be written as

$$\left(\tau + \frac{\partial \tau}{\partial z} dz\right) A - \tau A - \rho A dz \frac{\partial^2 U}{\partial t^2} = 0 \tag{2.24}$$

Here, U (t, z) is ground displacement in the horizontal direction induced by S-wave propagation, and is a function of time t and vertical coordinate z. A and dz

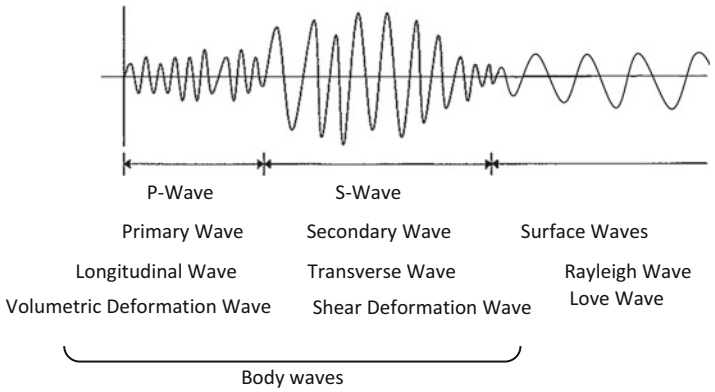

Fig. 2.16 Seismic waves

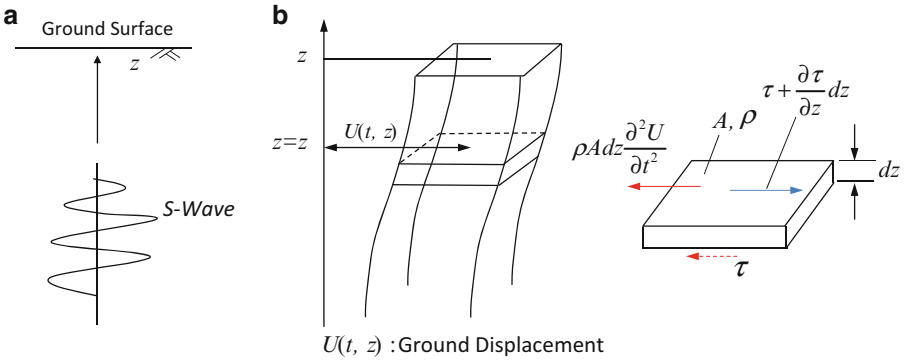

Fig. 2.17 Propagation of S-wave and wave equation. (**a**) Propagation of S-wave. (**b**) Force equilibrium of a soil segment

are area and thickness of the soil segment, and ρ is soil density. τ is the shear stress on the segment, and is expressed below using shear strain $\partial U/\partial z$.

$$\tau = G\frac{\partial U}{\partial z} \tag{2.25}$$

Here, G is the shear elastic modulus of the soil.
Assuming that G is constant, the following is obtained:

$$\frac{\partial^2 U}{\partial t^2} - {\nu_s}^2 \frac{\partial^2 U}{\partial z^2} = 0 \tag{2.26}$$

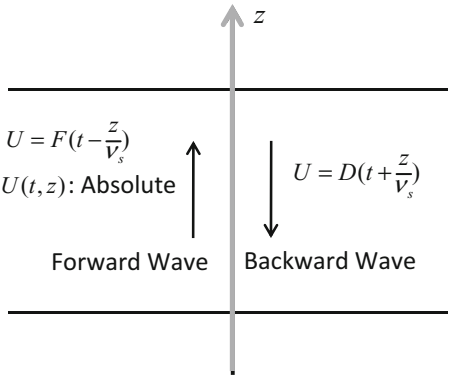

Fig. 2.18 Forward and backward waves

where ν_s is

$$\nu_s = \sqrt{\frac{G}{\rho}} \tag{2.27}$$

This indicates the propagation speed (called phase velocity).
A general solution satisfying Eq. (2.26) is shown below:

$$U(t,z) = F\left(t - \frac{z}{\nu_s}\right) \tag{2.28}$$

$$U(t,z) = D\left(t + \frac{z}{\nu_s}\right) \tag{2.29}$$

These two solutions show the waves propagating in plus and minus directions on the z axis, respectively. The wave represented by Eq. (2.28) is propagating in the plus direction and is called the forward wave. The wave represented by Eq. (2.29) is propagating in the minus direction, and is called the backward wave (Fig. 2.18).

Figure 2.19 depicts the response of surface ground with thickness H when bedrock motion $y(t)$ is input. Absolute displacement of the ground $U(t, z)$ is the sum of relative displacement $u(t, z)$ from the bedrock and displacement of the bedrock $y(t)$.

$$U(t,z) = u(t,z) + y(t) \tag{2.30}$$

Therefore, Eq. (2.26) is rewritten as

$$\frac{\partial^2 u}{\partial t^2} - {\nu_s}^2 \frac{\partial^2 u}{\partial z^2} = -\frac{d^2 y}{dt^2} \tag{2.31}$$

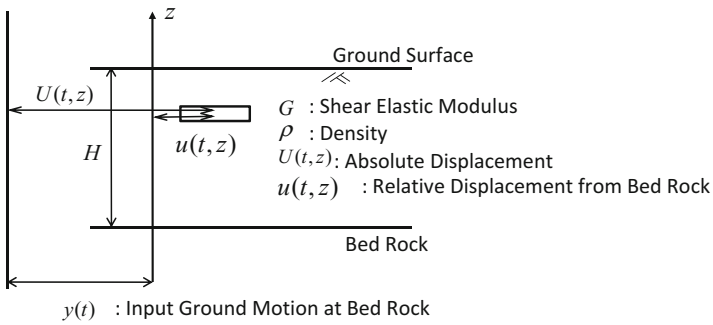

Fig. 2.19 Dynamic response of surface ground

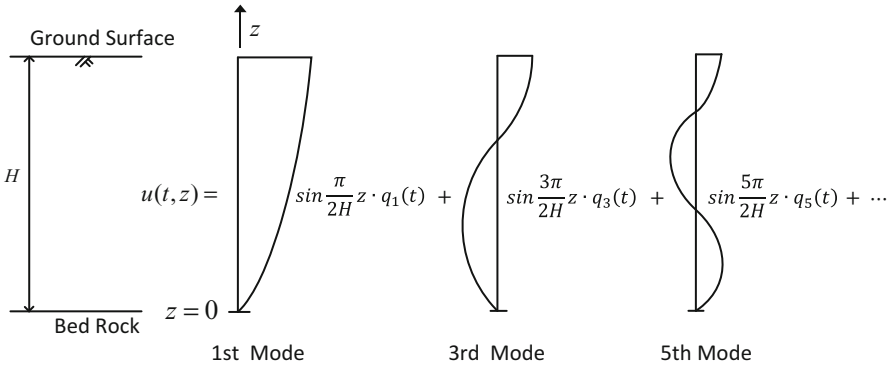

Fig. 2.20 Natural vibration modes

Equation (2.31) can be solved as below. The solution $u(t, z)$ is

$$u(t,z) = \sum_{i=1,3,5\cdots}^{\infty} q_i(t) \cdot \sin \frac{i\pi}{2H} z \tag{2.32}$$

In the above equation, $\sin \frac{i\pi}{2H} z$ is the ith vibration mode as illustrated in Fig. 2.20. Any vibration mode satisfies the boundary condition that the displacement $u(t, z)$ is zero at $z = 0$, and shear stress and shear strain are zero at $z = H$ (at the ground surface). $q_i(t)$ is the time function of the ith vibration.

By substituting Eq. (2.32) into Eq. (2.31), the following can be obtained:

$$\sum_{i=1,3,5\cdots}^{\infty} \ddot{q}_i(t) \cdot \sin \frac{i\pi}{2H} z + {v_s}^2 \sum_{i=1,3,5\cdots} \left(\frac{i\pi}{2H}\right)^2 q_i(t) \cdot \sin \frac{i\pi}{2H} z = -\frac{d^2 y}{dt^2} \tag{2.33}$$

By multiplying $\sin\frac{j\pi}{2H}z$ with the above equation and integrating from $z = 0$ to $2H$, the following can be attained by orthogonality of the trigonometric function, after replacing i with j:

$$\ddot{q}_i(t) + \omega_i^2 q_i(t) = -\frac{4}{i\pi}\frac{d^2y}{dt^2} \tag{2.34}$$

In the above equation, ω_i is the natural circular frequency of the ith vibration mode, as obtained below:

$$\omega_i = \frac{i\nu_s\pi}{2H} \qquad i = 1, 3, 5\cdots \tag{2.35}$$

The natural period of the ith vibration mode, T_i can be obtained from

$$T_i = \frac{4H}{i\nu_s} \qquad i = 1, 3, 5\cdots \tag{2.36}$$

Here, $i = 1$, that is, the first natural period $T_1 = 4H/\nu_s$ often appears as the dominant period of recorded earthquake ground motions. Because the soil has damping, the following is obtained by considering the damping term with respect to Eq. (2.34):

$$\ddot{q}_i(t) + 2\omega_i h_i \dot{q}_i(t) + \omega_i^2 q_i(t) = -\frac{4}{i\pi}\frac{d^2y}{dt^2} \tag{2.37}$$

Here, h_i is the critical damping constant regarding the ith vibration mode.

If the surface ground is composed by multiple soil layers of variable elastic shear modulus and density (Fig. 2.21a), the following simplified two methods are proposed for calculation of the natural periods of the surface ground:

$$T = \frac{4\sum_{i=1}^{n} H_i}{\overline{\nu}_s} \tag{2.38}$$

Here, $\overline{\nu}_s$ can be obtained as a mean of S-wave velocity, weighted by thickness of each soil layer.

$$\overline{\nu}_s = \frac{\sum_{i=1}^{n} H_i\nu_{si}}{\sum_{i=1}^{n} H_i} \tag{2.39}$$

Here, T is the natural period of the surface ground and H_i is thickness of the ith layer.

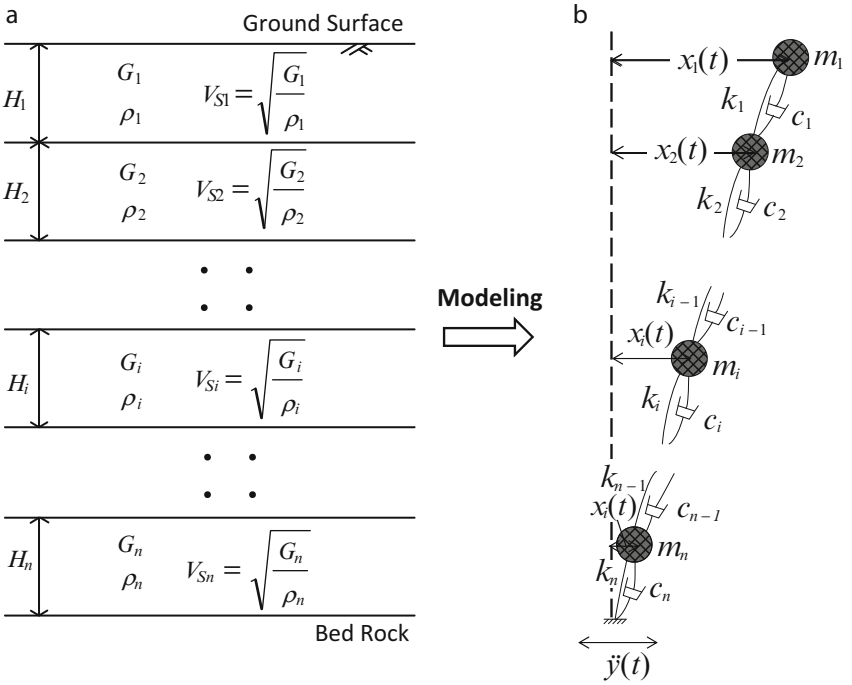

Fig. 2.21 Surface ground with multi-soil layers and mass-spring-damper model. (**a**) Surface ground with multi-soil layer. (**b**) Mass-spring-damper model

ν_{si} is S-wave velocity of ith soil layer, and is obtained by

$$\nu_{si} = \sqrt{\frac{G_i}{\rho_i}} \tag{2.40}$$

Here, G_i and ρ_i are shear elastic modulus and density, respectively.

The following equation is also a simple method for determining the natural period of the surface ground:

$$T = \sum_{i=1}^{n} \frac{4H_i}{\nu_{si}} \tag{2.41}$$

In "Specification for Highway Bridges and Explanation, Part V, Seismic Design," [3], a method to determine soil condition type by a characteristic value T_G representing the natural period of the surface ground is proposed. The ground condition is classified into the following groups:

soil condition I: T_G<0.2 s
soil condition II: 0.2 s < T_G < 0.6 s
soil condition III: 0.6 s < T_G

2.4.3 Dynamic Analysis by the Mass-Spring-Damper Model

Supported by the advancement of computing capacity since the 1970s, dynamic response analysis methods of structures and ground have been developed for use in earthquake-resistant design. Figure 2.21b shows multi-masses-springs-dampers model of surface ground composed by multiple soil layers. The vibration equation of this model can be generally expressed as follows:

$$\begin{bmatrix} m_1 & & & \\ & m_2 & 0 & \\ & 0 & & \\ & & & m_n \end{bmatrix} \begin{Bmatrix} \ddot{x}_1(t) \\ \ddot{x}_2(t) \\ \\ \ddot{x}_n(t) \end{Bmatrix} + \begin{bmatrix} c_1 & -c_1 & & \\ -c_1 & c_1 + c_2 & 0 & \\ & 0 & & \\ & & & c_{n-1} + c_n \end{bmatrix} \begin{Bmatrix} \dot{x}_1(t) \\ \dot{x}_2(t) \\ \\ \dot{x}_n(t) \end{Bmatrix}$$
$$+ \begin{bmatrix} k_1 & -k_1 & & \\ -k_1 & k_1 + k_2 & 0 & \\ & 0 & & \\ & & & k_{n-1} + k_n \end{bmatrix} \begin{Bmatrix} x_1(t) \\ x_2(t) \\ \\ x_n(t) \end{Bmatrix} = \begin{bmatrix} m_1 & & & \\ & m_2 & 0 & \\ & 0 & & \\ & & & m_n \end{bmatrix} \begin{Bmatrix} 1 \\ 1 \\ \\ 1 \end{Bmatrix} \ddot{y}(t) \tag{2.42}$$

In the above equation, $x_i(t)$, $\dot{x}_i(t)$, and $\ddot{x}_i(t)$ are relative displacement, relative velocity, and relative acceleration of the ith mass from the bedrock, and $\ddot{y}(t)$ represents the input acceleration on the bedrock. m_i is mass of the ith mass point, c_i, and k_i are viscous damping coefficient and spring constant that link the mass point i and mass point i + 1, respectively. Constants of m_i and k_i can be obtained as follows:

$$\begin{aligned} m_i &= \frac{1}{2}(\rho_{i-1}H_i + \rho_i H_i) \cdot A \\ k_i &= \frac{G_i A}{H_i} \end{aligned} \tag{2.43}$$

Here, A is area of the soil column, and usually takes as unit, and G_i and H_i is the elastic shear modulus and the thickness of ith layer.

c_i is the viscous damping constant between the ith mass and (i + 1)th mass. This coefficient usually is presumed proportional to the mass m_i or the spring constant k_i.

The matrixes $\boldsymbol{M}$, $\boldsymbol{C}$, $\boldsymbol{K}$ and the vector $\boldsymbol{X}$ are defined as follows,

$$\boldsymbol{M} = \begin{bmatrix} m_1 & & & & & \\ & m_2 & & 0 & & \\ & & \ddots & & & \\ & & & m_i & & \\ & 0 & & & \ddots & \\ & & & & & m_n \end{bmatrix} \quad \boldsymbol{C} = \begin{bmatrix} c_1 & -c_1 & & & & \\ -c_1 & c_1 + c_2 & & & 0 & \\ & & \ddots & & & \\ & & & \ddots & & \\ & 0 & & & \ddots & \\ & & & & & c_{n-1} + c_n \end{bmatrix}$$

$$\boldsymbol{K} = \begin{bmatrix} k_1 & -k_1 & & & \\ -k_1 & k_1 + k_2 & & 0 & \\ & & \ddots & & \\ & & & \ddots & \\ & 0 & & & \ddots \\ & & & & k_{n-1} + k_n \end{bmatrix} \quad \boldsymbol{X} = \begin{Bmatrix} x_1 \\ x_2 \\ \vdots \\ x_n \end{Bmatrix} \tag{2.44}$$

Equation (2.45) can be obtained:

$$\boldsymbol{M} \cdot \ddot{\boldsymbol{X}} + \boldsymbol{C} \cdot \dot{\boldsymbol{X}} + \boldsymbol{K} \cdot \boldsymbol{X} = -\boldsymbol{M} \cdot \boldsymbol{1} \cdot \ddot{y}(t) \quad \boldsymbol{1} = \begin{Bmatrix} 1 \\ 1 \\ \vdots \\ 1 \end{Bmatrix} \tag{2.45}$$

With respect to Eq. (2.45), $\boldsymbol{M}$, $\boldsymbol{C}$, and $\boldsymbol{K}$ are mass, damping and stiffness matrices, respectively. In addition, $\ddot{\boldsymbol{X}}$, $\dot{\boldsymbol{X}}$ and $\boldsymbol{X}$ are acceleration, velocity, and displacement vectors, respectively. $\boldsymbol{1}$ is the vector whose elements are all 1.

The following three methods are used to solve Eq. (2.45) under a given input acceleration $\ddot{y}(t)$ at the bedrock: (i) Direct integration in time domain; (ii) Integration in frequency domain by Fourier transformation; and (iii) Modal analysis.

For an analysis in which nonlinear characteristics of the material property of the soil or structures are considered, the direct integration in time domain is generally used.

2.4.3.1 Direct Integration in Time Domain

Under the condition in which $\boldsymbol{X}(t_{j-1})$ and $\boldsymbol{X}(t_j)$ are given at $t = t_{j-1}$ and $t = t_j$, $\boldsymbol{X}(t_{j+1})$ can be obtained by the following procedure (Fig. 2.22). For a constant time interval Δt, the velocity vector $\dot{\boldsymbol{X}}(t_j)$ can be expressed as

$$\dot{\boldsymbol{X}}(t_j) = \left[\boldsymbol{X}(t_{j+1}) - \boldsymbol{X}(t_j)\right]/\Delta t \tag{2.46}$$

Likewise, the acceleration vector $\ddot{\boldsymbol{X}}(t_j)$ is

$$\ddot{\boldsymbol{X}}(t_j) = \left[\boldsymbol{X}(t_{j+1}) + \boldsymbol{X}(t_{j-1}) - 2\boldsymbol{X}(t_j)\right]/\Delta t^2 \tag{2.47}$$

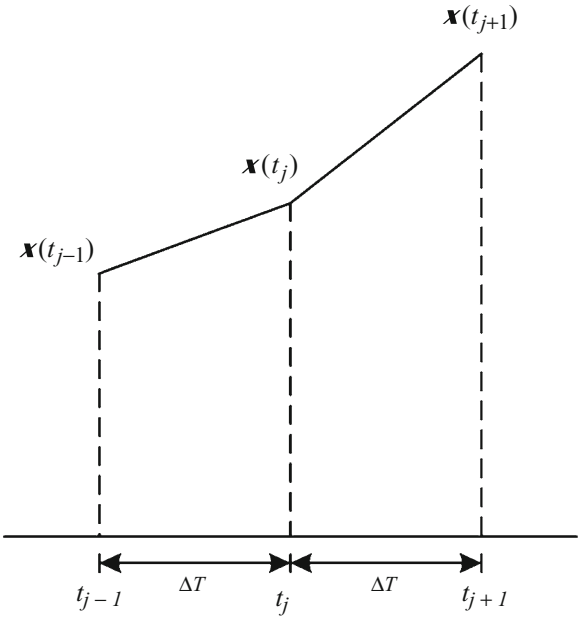

Fig. 2.22 Solution of vibration equation by direct integration method

By substituting Eqs. (2.46) and (2.47) into Eq. (2.44), the following is obtained:

$$\begin{aligned}\boldsymbol{M}\cdot\lfloor\boldsymbol{X}(t_{j+1})+\boldsymbol{X}(t_{j-1})-2\boldsymbol{X}(t_j)\rfloor/\Delta t^2+\boldsymbol{C}\cdot\lfloor\boldsymbol{X}(t_{j+1})-\boldsymbol{X}(t_j)\rfloor/\Delta t\\+\boldsymbol{K}\cdot\boldsymbol{X}(t_j)=-\boldsymbol{M}\cdot\boldsymbol{1}\cdot\ddot{y}(t_j)\end{aligned}\tag{2.48}$$

When $\boldsymbol{X}(t_{j-1})$, $\boldsymbol{X}(t_j)$, and input acceleration $\ddot{y}(t_j)$ at time of t_j are given, $\boldsymbol{X}(t_{j+1})$ can be attained. Repeating this procedure, the time history of $\boldsymbol{X}(t)$ is acquired.

2.4.3.2 Integration in Frequency Domain by Fourier Transformation

Fourier transformation $X_i(\omega)$ of the ith element $x_i(t)$ of the displacement vector $\boldsymbol{X}(t)$ is

$$X_i(\omega)=\int_{-\infty}^{\infty}x_i(t)\cdot e^{-i\omega t}\cdot d\omega\tag{2.49}$$

It therefore follows that Fourier transformation $\boldsymbol{X}_F(\omega)$ of the displacement vector $\boldsymbol{X}(t)$ becomes

$$\boldsymbol{X}_F(\omega)=\begin{Bmatrix}X_1(\omega)\\X_2(\omega)\\\vdots\\X_n(\omega)\end{Bmatrix}\tag{2.50}$$

Fourier transformation of the velocity vector $\dot{\boldsymbol{X}}(t_j)$ and acceleration vector $\ddot{\boldsymbol{X}}(t_j)$ are expressed as

$$-i\omega \boldsymbol{X}_F(\omega) \tag{2.51}$$
$$-\omega^2 \boldsymbol{X}_F(\omega)$$

Therefore, Fourier transformation of Eq. (2.45) can be done as

$$-\omega^2 \boldsymbol{M} \cdot \boldsymbol{X}_F(\omega) - i\omega \cdot \boldsymbol{C} \cdot \boldsymbol{X}_F(\omega) + \boldsymbol{K} \cdot \boldsymbol{X}_F(\omega) = -\boldsymbol{M} \cdot \boldsymbol{1} \cdot Y(\omega) \tag{2.52}$$

Here, $Y(\omega)$ is Fourier transformation of the input acceleration $\ddot{y}(t)$
From Eq. (2.52), the following can be obtained:

$$\boldsymbol{X}_F(\omega) = \left[\omega^2 \boldsymbol{M} + i\omega \cdot \boldsymbol{C} - \boldsymbol{K}\right]^{-1} \cdot \boldsymbol{M} \cdot \boldsymbol{1} \cdot Y(\omega) \tag{2.53}$$

Here, x_i(t) is displacement of ith element of vector $\boldsymbol{X}(t)$, which can be attained by inverse transformation $X_i(\omega)$, as shown below:

$$x_i(t) = \frac{1}{2\pi} \int_{-\infty}^{\infty} X_i(\omega) \cdot e^{i\omega t} \cdot d\omega \tag{2.54}$$

2.4.3.3 Modal Analysis

The equation of free vibration in which both the damping term and input motion $y(t)$ are zero, can be written from Eq. (2.45), as follows.

$$\boldsymbol{M} \cdot \ddot{\boldsymbol{x}} + \boldsymbol{K} \cdot \boldsymbol{x} = \boldsymbol{0} \tag{2.55}$$

Here $\boldsymbol{0}$ is a vector, all elements of which are zero.
When the displacement vector $\boldsymbol{x}(t)$ is written as

$$\boldsymbol{x} = \boldsymbol{X} \cdot e^{iwt} \tag{2.56}$$

the following is obtained:

$$-\omega^2 \cdot \boldsymbol{M} \cdot \boldsymbol{X} + \boldsymbol{K} \cdot \boldsymbol{X} = \boldsymbol{0} \tag{2.57}$$

where $\boldsymbol{X}$ expresses the vibration mode of the free vibration, and ω is circular frequency. Eq. (2.57) is rewritten as

$$\omega^2 \cdot \boldsymbol{X} = \boldsymbol{M}^{-1} \boldsymbol{K} \cdot \boldsymbol{X} \tag{2.58}$$

Thus, this becomes the eigenvalue problem of matrix $\boldsymbol{M}^{-1}\boldsymbol{K}$.

Different n values of ω satisfying Eq. (2.58) are attained, and vector $\boldsymbol{X}$ (vibration mode) is obtained as shown below.

$$\begin{array}{llll} 1st & \text{vibration} & \omega_1 & X_{11}, X_{21} \ldots\ldots\ldots\ldots X_{\mathrm{n}1} \\ ith & \text{vibration} & \omega_{\mathrm{i}} & X_{1i}, X_{2i} \ldots\ldots\ldots\ldots X_{ni} \\ \mathrm{n}th & \text{vibration} & \omega_{\mathrm{n}} & X_{1n}, X_{2n} \ldots\ldots\ldots\ldots X_{nn} \end{array} \tag{2.59}$$

In the above equation, X_{ji} expresses the vibration mode value of the jth mass of the ith vibration. The ith vibration mode is

$$\boldsymbol{X}_i = \begin{Bmatrix} X_{1i} \\ X_{2i} \\ \vdots \\ X_{ni} \end{Bmatrix} \tag{2.60}$$

$\boldsymbol{X}_i$ satisfies the following equation:

$$-\omega_i^2 \cdot \boldsymbol{M} \cdot \boldsymbol{X}_i + \boldsymbol{K} \cdot \boldsymbol{X}_i = \boldsymbol{0} \tag{2.61}$$

Likewise, the jth vibration mode $\boldsymbol{X}_j$ satisfies the following:

$$-\omega_j^2 \cdot \boldsymbol{M} \cdot \boldsymbol{X}_j + \boldsymbol{K} \cdot \boldsymbol{X}_j = \boldsymbol{0} \tag{2.62}$$

By multiplying Eq. (2.61) by the transpose vector $\boldsymbol{X}_j^T$ and Eq. (2.62) by transpose vector $\boldsymbol{X}_i^T$ the following is obtained:

$$-\omega_i^2 \boldsymbol{X}_j^T \cdot \boldsymbol{M} \cdot \boldsymbol{X}_i + \boldsymbol{X}_j^T \cdot \boldsymbol{K} \cdot \boldsymbol{X}_i = \boldsymbol{0} \tag{2.63}$$

$$-\omega_i^2 \boldsymbol{X}_i^T \cdot \boldsymbol{M} \cdot \boldsymbol{X}_j + \boldsymbol{X}_i^T \cdot \boldsymbol{K} \cdot \boldsymbol{X}_j = \boldsymbol{0} \tag{2.64}$$

where each of $\boldsymbol{X}_j^T \cdot \boldsymbol{K} \cdot \boldsymbol{X}_i$ and $\boldsymbol{X}_i^T \cdot \boldsymbol{K} \cdot \boldsymbol{X}_j$ is scalar. Therefore, the following are attained:

$$\left(\boldsymbol{X}_j^T \cdot \boldsymbol{K} \cdot \boldsymbol{X}_i\right)^T = \boldsymbol{X}_j^T \cdot \boldsymbol{K} \cdot \boldsymbol{X}_i \tag{2.65}$$

$$\boldsymbol{X}_i^T \cdot \boldsymbol{K}^T \cdot \boldsymbol{X}_j = \boldsymbol{X}_j^T \cdot \boldsymbol{K} \cdot \boldsymbol{X}_i \tag{2.66}$$

Because stiffness matrix $\boldsymbol{K}$ is symmetric,

$$\boldsymbol{X}_i^T \cdot \boldsymbol{K} \cdot \boldsymbol{X}_j = \boldsymbol{X}_j^T \cdot \boldsymbol{K} \cdot \boldsymbol{X}_i \tag{2.67}$$

Likewise, because mass matrix $\boldsymbol{M}$ is diagonal, the following is obtained:

$$\boldsymbol{X}_i^T \cdot \boldsymbol{M} \cdot \boldsymbol{X}_j = \boldsymbol{X}_j^T \cdot \boldsymbol{M} \cdot \boldsymbol{X}_i \tag{2.68}$$

Subtracting Eq. (2.64) from Eq. (2.63) produces

$$\left(\omega_j^2 - \omega_i^2\right) \cdot \boldsymbol{X}_j^T \cdot \boldsymbol{M} \cdot \boldsymbol{X}_i = 0 \tag{2.69}$$

where $\omega_i \neq \omega_j$; that is, if i≠j, the following is obtained:

$$\boldsymbol{X}_j^T \cdot \boldsymbol{M} \cdot \boldsymbol{X}_i = 0 \tag{2.70}$$

This is called orthogonal condition of the vibration mode. Likewise, we obtain

$$\boldsymbol{X}_j^T \cdot \boldsymbol{K} \cdot \boldsymbol{X}_i = 0 \tag{2.71}$$

The modal analysis method solves a partial differentiation equation using orthogonal condition among the vibration modes. The solution of Eq. (2.45) is

$$[\boldsymbol{X}] = [\,\boldsymbol{X}_1 \quad \boldsymbol{X}_2 \ldots \boldsymbol{X}_i \ldots \boldsymbol{X}_n\,] \cdot \begin{Bmatrix} q_1(t) \\ q_2(t) \\ \vdots \\ q_i(t) \\ \vdots \\ q_n(t) \end{Bmatrix} \tag{2.72}$$

where $\boldsymbol{X}_i$ is the ith vibration mode, and $q_i(t)$ is a time function relating to the ith vibration. Suppose that damping matrix $\boldsymbol{C}$ is proportional for mass matrix $\boldsymbol{M}$ or stiffness matrix $\boldsymbol{K}$. By substituting Eq. (2.72) into Eq. (2.45) and by orthogonal condition of the vibration mode mentioned above, the following is obtained.

$$\ddot{q}_i + 2\omega_i h_i \dot{q}_i + \omega_i^2 q_i = -\frac{\boldsymbol{X}_i^T \cdot \boldsymbol{M} \cdot \boldsymbol{1}}{\boldsymbol{X}_i^T \cdot \boldsymbol{M} \cdot \boldsymbol{X}_i} \ddot{y}(t) \tag{2.73}$$

In the above equation, h_i is the critical damping constant regarding the ith vibration. Provided the damping matrix $\boldsymbol{C}$ is given, the critical damping constant can be calculated. However, h_i corresponding to each vibration mode is directly determined in all general cases. Using masses m_1 to m_n of the individual mass, the right side of Eq. (2.73) is

$$-\frac{\boldsymbol{X}_i^T \cdot \boldsymbol{M} \cdot \boldsymbol{1}}{\boldsymbol{X}_i^T \cdot \boldsymbol{M} \cdot \boldsymbol{X}_i} \ddot{y}(t) = -\frac{\sum_{j=1}^{n} m_j X_{ji}}{\sum_{j=1}^{n} m_j X_{ji}^2} \ddot{y}(t) \tag{2.74}$$

The fraction on the right side is called a excitation function of the vibration mode. A vibration mode with larger excitation function has greater influence on vibration of the mass-spring –damper model. Eq. (2.73) is the same as that of the dynamic response of the single mass-spring-damper model shown in Eq. (2.7). Provided the input earthquake motion $\ddot{y}(t)$ is given, the time history of $q_i(t)$ can be attained. Furthermore, substituting $q_i(t)$ of Eq. (2.73) into Eq. (2.72) makes it possible for vector $\boldsymbol{X}(t)$ of the time history of response displacement to be calculated.

2.5 Seismic Reinforcement

The Japan Society of Civil Engineers (JSCE) recommended the followings with respect to seismic diagnosis and reinforcement of existing civil engineering structures after the 1995 Kobe earthquake. The first recommendation stated "Keeping the experience of disaster caused by the Kobe earthquake in mind, seismic diagnosis of existing structures shall be promoted in order of importance, and necessary reinforcement shall be rapidly promoted" [8]. The second recommendation states "The aim of seismic reinforcement shall be the same as that of newly built structures, and studies and development concerning seismic diagnosis and reinforcement technology shall be promoted."

The third recommendation of the Japan Institute of Architecture (AIJ) also indicates the "...importance of development of technologies for diagnosis and reinforcement of historical buildings and existing structures that do not satisfy the current standard of earthquake resistance. AIJ also indicates the necessity of investment and social alignment for retrofitting." Furthermore, the *Basic Disaster Prevention Plan* [9], revised in July 1995, states that "Enhancement of earthquake resistance of major infrastructures based on damage assessment should be dealt with as an important subject in the future."

Based on these recommendations, earthquake-resistant reinforcement has been carried out on infrastructures such as bridges, subways, quay walls, road and railway embankments, and with various types of lifelines. In this section, this reinforcement is described mainly with respect to civil engineering structures. Reinforcement of ground and foundations against soil liquefaction and liquefaction-induced ground displacements are introduced in Sects. 3.3 and 4.4.

2.5.1 Seismic Reinforcement of Concrete Piers

Considering the destruction of concrete piers by the 1995 Kobe earthquake, earthquake-resistant reinforcement of about 16,000 piers of road bridges, railway viaducts, subways and other structures was executed after the earthquake. Reinforcement of concrete piers was done by steel plate jacketing (Fig. 2.23a) or new

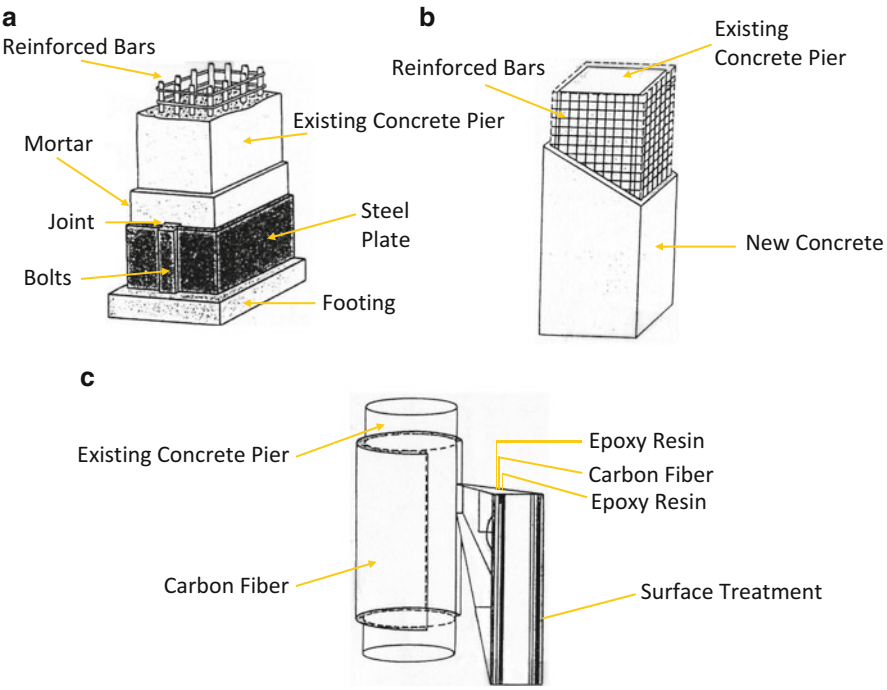

Fig. 2.23 Reinforcement of concrete piers. (**a**) Steel plate jacketing. (**b**) New concrete casting. (**c**) Carbon fiber facing

concrete casting (Fig. 2.23b). Examples of the reinforcement of viaducts of the Shinkansen (new trunk line), center columns of a subway, and piers of an express highway are shown in Fig. 2.24. Shear failures of subway center columns resulted in total collapse in Kobe. Therefore, about 3,000 concrete subway columns were reinforced in big cities, such as Tokyo and Osaka. In addition to the above-mentioned two methods, reinforcement by aramid and carbon fibers (Fig. 2.23c), and PC steel bars have been adopted. Furthermore, for rigid-frame piers, methods to construct shear walls between the piers and methods using dampers have been developed. The effectiveness of concrete pier reinforcement by steel jacketing was examined by model tests. It was confirmed that both strength and ductility of reinforced piers increased.

2.5.2 Seismic Reinforcement of Earth Dams

Niteko Reservoir dam in Nishinomiya slid and sank significantly in the 1995 Kobe earthquake (Fig. 2.25). N-values of the dam body and foundation ground were less than 10, and circular slip was caused by strong earthquake motion near the

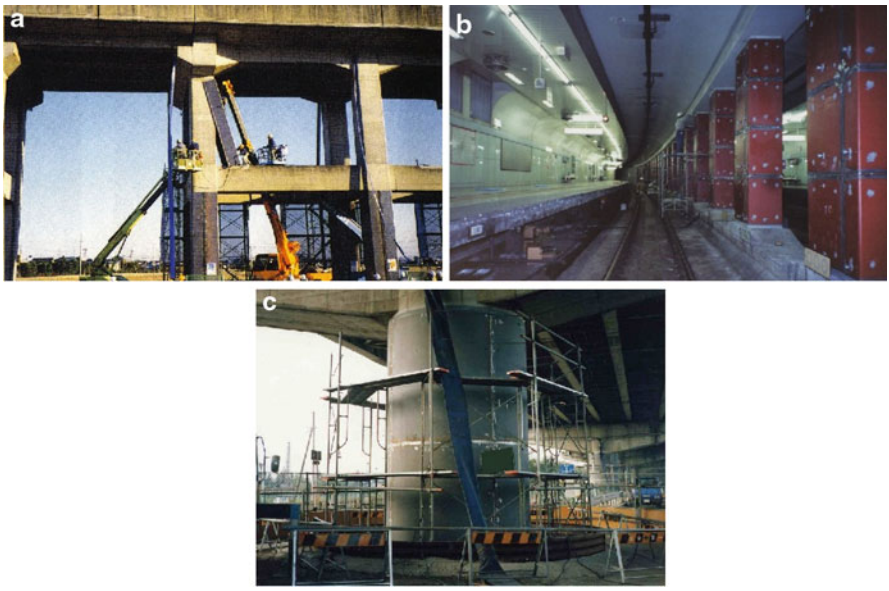

Fig. 2.24 Seismic reinforcement of concrete structures (by steel jacketing). (**a**) Concrete viaduct of shinkansen (*new trunk line*). (**b**) Center concrete column of subway station. (**c**) Concrete bridge pier of a express way

Fig. 2.25 Slide and sinkage of Niteko earth dam (1995 Kobe earthquake)

active fault. The dam was located in a densely populated area and had height approximately 15 m. Fortunately, the water level of the reservoir at the time of the earthquake was low, so there was no flooding.

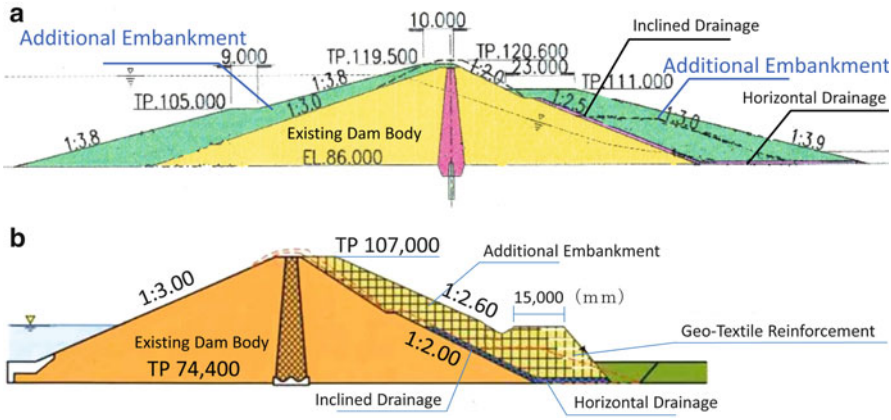

Fig. 2.26 Reinforcement of earth dams (Tokyo bureau of waterworks). (**a**) Yamaguchi reservoir (additional embankment). (**b**) Murayama reservoir (additional embankment and geo-textile reinforcement)

Motivated by such damage to the dam, the Tokyo Bureau of Waterworks conducted seismic reinforcement of two earth dams, at Yamaguchi (Sayama Lake) and Murayama (Tama Lake) reservoirs by methods illustrated in Fig. 2.26 [13]. The heights of Yamaguchi and Murayama dams are 34.6and 32.6 m, respectively. When dam construction began, surrounding areas were forested, but residential areas have been gradually developed. In particular, the downstream area had been rapidly populated. Therefore, dam safety should be ensured to protect life and property of people against level 2 earthquake ground motion that is predicted to be caused by nearby faults.

Each dam was reinforced by additional embankments on their surfaces to enhance safety against surface sliding. As illustrated in Fig. 2.26a, embankments were added on both upstream and downstream sides of Yamaguchi dam. Embankments were added on the downstream surface of Murayama dam. Furthermore, a method to reinforce the end of a slope with geotextiles was used (Fig. 2.26b), because the end of the embankment abuts parkland. The added embankment increases effective stress of the dam and thereby ensure the safety against slope sliding failure.

2.6 Measures Against Surface Earthquake Faults

There are more than 2,000 active faults in Japan. With particular regard to the 98 fault belts with relatively high activity, the Headquarters for Earthquake Research Promotion of the Ministry of Education, Culture, Sports, Science and Technology (MEXT) is engaged in a continuous survey of this fault belts. An active fault in the earth crust whose failure emerges at the surface is called a surface

Table 2.3 Earthquake faults (1981–1995)

Year	Earthquake	Faults	Fault offset	
			V: vertical (m)	H: horizontal (m)
1981	Nobi	Neodani	4.0	6.0
1896	Rikuu	Senya faults	3.5	–
1923	Kanto	Enmaiji	1.9	1.2
1925	Tajima	Tai	1.0	–
1927	Northern-Tango	Atomura	0.5	3.0
1930	Northern-Izu	Tanna	1.8	3.5
1938	Kussharo	Kussharo	0.9	2.6
1943	Tottori	Shikano	0.5	1.5
1945	Mikawa	Fukamizu	2.0	1.3
1948	Fukui	Fukui	0.7	2.0
1978	Izu Oshima offshore	Inatori-Omineyama	0.36	1.15
1995	Kobe	Nojima	1.6	1.8

earthquake fault or simply an earthquake fault. Examples of earthquake faults in Japan over 130 years are shown in Table 2.3. Among these, the 1891 Nobi earthquake caused the greatest surface fault. The Neodani Fault appeared on the surface, producing a 6.0 m offset in the horizontal and 4.0 m in the vertical. In the 1995 Kobe earthquake, the fault offset at Hokutan in Awaji Island was 1.8 m in the horizontal and 1.6 m in the vertical. Globally, many earthquake faults have appeared at the ground surface, destroying structures. In the 1999 Kocaeli (Turkey) earthquake, concrete girders of a bridge crossing an earthquake fault collapsed (Sect. 1.2.1). In the 1999 Chi-Chi earthquake, Taiwan, a concrete dam of height 25 m was destroyed by a 10 m differential displacement in the vertical direction from a reverse fault (Sect. 1.2.2). Fortunately, there are no known examples of direct damage to important structures by surface earthquake faults in Japan.

However, in the 1930 Northern-Izu earthquake (Table 2.3), faults crossed Tanna tunnel of the Tokaido Railway Line, which was under construction. The tunnel excavation face was completely lost. Furthermore, in the 1978 Off-Izu Oshima earthquake, the Inatori-Omineyama Fault crossed Inatori Tunnel, destroying the lining. It was reported that a large amount of soil entered the tunnel. The rail was lifted 50 cm, and meandered about 50 cm in the horizontal [14].

What measures should be taken to protect important structures against earthquake faults? Definitive countermeasures are exceedingly difficult but few have been realized. An example of such countermeasures for earthquake faults is Fuji River Bridge of the Tokaido Shinkansen (new trunk line). Near the Fuji River is Iriyamase Fault, with a high activity degree. Based on the supposition that this fault will move during the predicted Tokai earthquake, the effect on the bridge was examined. By surmising the amount of fault movement, damage to the truss bridge members was numerically analyzed. Based on this analysis, the top of a pier was expanded to prevent girders from falling (Fig. 2.27a). Together with this, preparatory members of the bridge and shoes that are presumed susceptible to be damaged

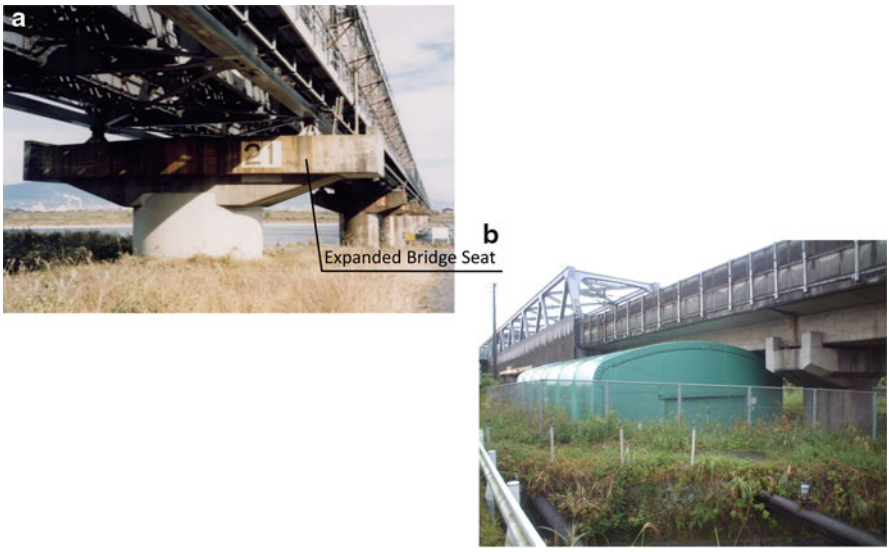

Fig. 2.27 Measures for Tokaido shinkansen against surface earthquake fault. (**a**) Expansion of bridge seat for prevention of girders' falling. (**b**) Storage of preparatory members of the truss bridge

were fabricated and kept in a hangar near the bridge (Fig. 2.27b). These measures are not aimed at operational safety of the high-speed train, but are intended for early recovery. It is difficult to ensure operational safety against earthquake faults directly beneath high-speed train like the Shinkansen. Particularly, safety is threatened wherever earthquake faults cross a tunnel.

Here is one more example of countermeasures for the Shinkansen against earthquake faults [15]. In construction of a viaduct of the platform of New-Kobe station of the Sanyo Shinkansen, an earthquake fault was found during excavation of foundation ground (Fig. 2.28). Through geologic survey, earthquake fault offset was shown to have exceeded 70 cm in the vertical during the last 10,000 years or so. To deal with the fault offset in the future, movable shoes were installed between the platform deck and viaduct. Furthermore, the floor slab of the platform and columns were connected by hinges. These countermeasures are intended to absorb vertical offset of the earthquake fault and rotational deformation. However, this cannot guarantee operational safety of the Shinkansen.

There are several examples of countermeasures to protect structures against surface earthquake faults in the world. One of the water supply sources of East Bay Municipal Utility District (EBMUD) in Oakland, USA, is Pardee Reservoir to the west of the city (Fig. 2.29a). A trunk line connects the reservoir with Oakland, which is crossed by the Hayward Fault in the Claremont Tunnel (Fig. 2.29b). Therefore, flexible pipes were used in the tunnel and shutdown valves were installed at its exits. Furthermore, temporary hoses were prepared for emergency water supply and stored in the neighborhood. In addition to these measures, EBMUD constructed a new trunk line, the South Trunk Line (Fig. 2.29a), to form a loop network for the water supply.

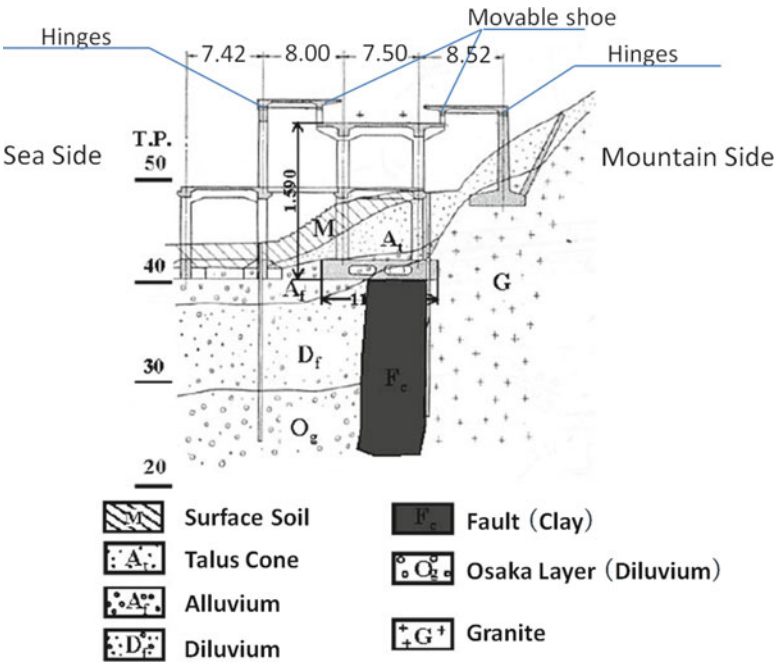

Fig. 2.28 Measures for new Kobe station of Sanyo shinkansen against earthquake faults [15]

These countermeasures are only possible when the location of the earthquake fault can be identified with high reliability. If surface ground is composed of thick soil, it is difficult to identify locations of earthquake faults in the bedrock.

Another example of countermeasures against earthquake faults is the case of Clyde Dam in the South Island of New Zealand, shown in Fig. 2.30, which is gravity-type concrete dam with a height of 102 m. Waterproof slip joints were installed in the dam body along the vertical direction. This joint can absorb 2 m fault offset in the horizontal and 1 m in the vertical [16].

2.7 Earthquake-Resistant Design of Nuclear Power Plants

2.7.1 Accident at the Fukushima Daiichi Nuclear Plant

The plan and concrete methods to end the serious accident at the Fukushima Daiichi Nuclear Power Plant are not yet decided at the time of this writing, but contamination by radioactive materials spread not only through Fukushima Prefecture but also over wide areas of Tohoku and Kanto regions. It is believed that it will take several 10 years to terminate this disaster.

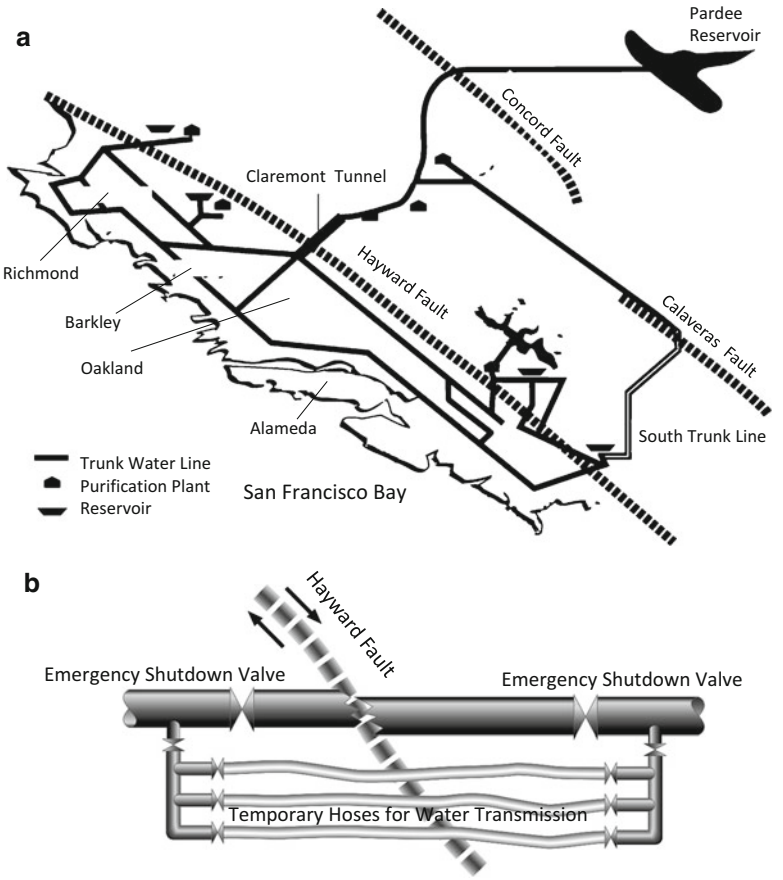

Fig. 2.29 Measure by EBMUD (East Bay Municipal Utility District) against earthquake fault. (**a**) Reinforcement of water transmission network by construction of south trunk line. (**b**) Emergency shutdown valves and temporary hoses

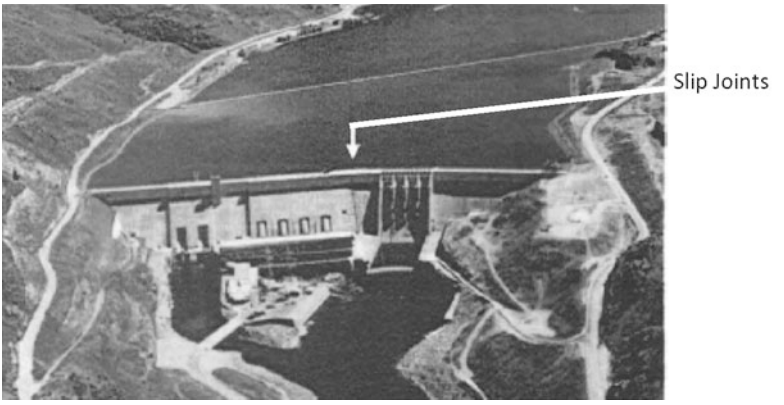

Fig. 2.30 Clyde dam with slip joints for absorbing of faults offset (height: 102 m, concrete dam)

Ensuring nuclear power plant safety in an emergency requires the following three major procedures [17].

(i) Ceasing the nuclear reaction
(ii) Cooling nuclear fuels to a cryogenic state
(iii) Confining radioactive materials in the nuclear reactor

Nuclear reaction at the Fukushima Daiichi Nuclear Power Plant was successfully halted by control-bar insertion in all reactors (Nos. 1 through 4) but all electric (including emergency) power sources were lost, triggering a hydrogen explosion. Thus, a large amount of radioactive material was emitted and dispersed. Concurrently, a large amount of contaminated water entered the sea, increasing the danger of contamination to fish and shellfish. A temporary cooling system for the nuclear reactor and fuel was constructed, in which radio active contamination of the water from the reactor was lowered and was returned to the reactor.

It is no exaggeration to say that the origin of the serious accident at the 1st Fukushima Nuclear Power Plant was due to the failure of tsunami prediction and countermeasures. It remains to be seen whether public confidence in atomic power can be restored for the continuance of nuclear power generation. To restore this confidence, it is necessary to fully comprehend why the prediction of tsunami height in the plant design was failed. Extensive examination of expected tsunamis is mandatory for the design of nuclear power plants. Taking necessary tsunami-resistant countermeasures during this examination is urgently required.

To maintain nuclear power generation in Japan, it is critical to have the concurrence of the public. To accomplish this, understandable explanations of the accident causes and exact information on tsunami-resistant countermeasures are essential.

In recent years, nuclear power generation has been promoted in underdeveloped countries, including in Asia. However, serious accidents have widespread and substantial effects. Safety of nuclear power plants against earthquakes and tsunamis must be inspected according to standards of individual countries and International Atomic Energy Agency (IAEA) guidelines. Japan, which unfortunately experienced the accident at the 1st Fukushima plant, is required to contribute to the improvement of earthquake and tsunami resistance of nuclear power plants based on its experience.

The author has long participated in inspecting earthquake resistance of nuclear power plants, as a member of the Nuclear Reactor Safety Inspection Committee of Japan. He has also taught earthquake-resistant engineering of nuclear facilities in a nuclear engineering course at a joint graduate school of Waseda University and Tokyo City University. The present state and problematic issues of earthquake-resistant design of nuclear power plants are introduced in this session.

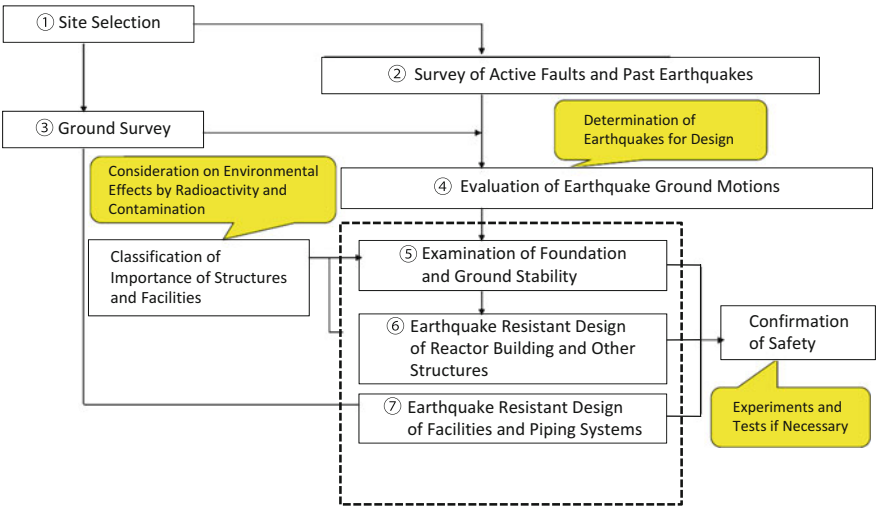

Fig. 2.31 Flow of earthquake resistant design of nuclear power plant

2.7.2 Flowchart of Earthquake-Resistant Design of Nuclear Power Plants and Surveys of Active Faults

A flowchart of the earthquake-resistant design of nuclear power plants is given in Fig. 2.31. In that chart, a survey of active faults and past earthquakes is required over a wide region to determine ground motions for the design. Referring to the literature about active faults in the plant surroundings, those faults affecting seismic safety of the plant are selected. In the next stage, lineament survey by air photos, outcrop observation, geologic survey by elastic and sound waves, and trench excavation are carried out. For geologic and soil conditions of the seabed near the plant, investigation is done mainly by sonic prospecting.

Nevertheless, it is generally difficult to detect all active faults that substantially affect seismic safety of the nuclear plant during the design stage. As mentioned in Sect. 1.3.5 and 1.3.8, active faults which caused the 2004 Niigata-Chuetsu and 2008 Iwate-Miyagi Inland earthquakes have not been recognized prion to earthquake occurrence.

Surveying active faults in sea regions is more difficult than on land, causing frequent misjudgment or oversight of such faults. The 2007 Niigata-Chuetsu offshore earthquake caused accidents such as electric transformer fire, overflow of cooling water from spent fuel tanks, and others. As illustrated in Fig. 1.84, earthquake ground motion observed on a reactor-building basement greatly exceeded the design motion. These facts impugn the reliability of active fault surveys for determining earthquake ground motions in the design.

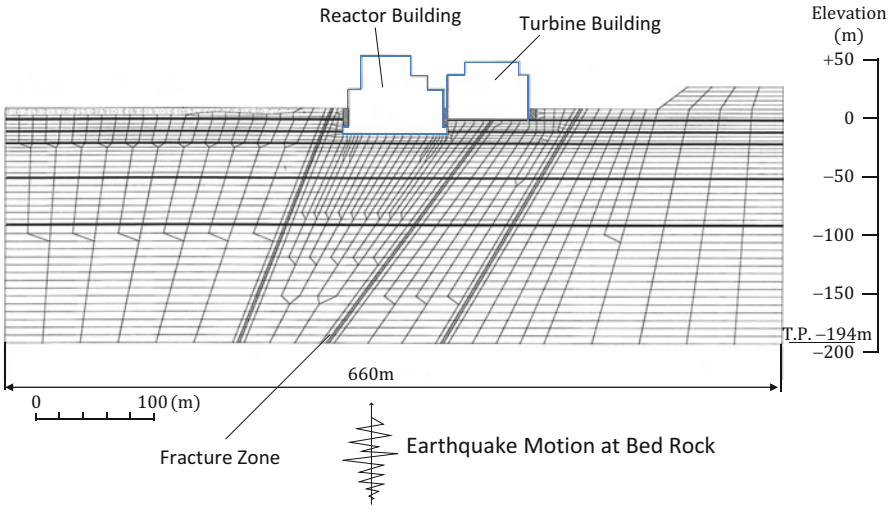

Fig. 2.32 Finite element model for dynamic analysis of foundation ground and building of nuclear power plant

Similar findings were reported in the 2007 Noto Peninsula earthquake. In design and construction of the Shika Nuclear Power Plant, active faults were identified (Fig. 1.79). However, the active fault that caused the earthquake was overlooked, but was identified after the event. Such oversight for two nuclear power plants highlights the difficulty of active fault surveys, particularly in sea regions.

2.7.3 Earthquake-Resistant Design of Structures, Facilities and Foundation Ground [17]

After selecting the active fault in earthquake-resistant design of the plant, earthquake motion on the bedrock is evaluated based on the magnitude of the fault, distance from the fault to the plant, and properties of the bedrock. Using the earthquake ground motion, the bedrock stability is examined with a finite element model (Fig. 2.32), in which fissures and weak seams are also modeled. The stiffness and strength of rock and weak seams are surveyed by in-situ and laboratory tests.

In the next stage, the dynamic response of structures such as reactor buildings is simulated, using bedrock motion as an input wave. Based on the simulation result, structure safety is examined and dynamic response of each floor of the structures is calculated for the design of facilities and piping on the floor.

For nuclear power plants, intake ducts for emergency cooling water, which allow the nuclear reactor to be submerged during serious accidents, are constructed.

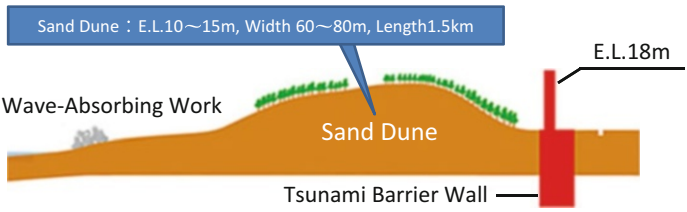

Fig. 2.33 Construction of tsunami barrier wall (Hamaoka nuclear power plant)

The intake ducts generally have a concrete box section, and steel pipes to take in water are installed inside the ducts. Earthquake-resistant design of these ducts is done by the response displacement method described in Sect. 5.6.

There are often slopes on the backsides of nuclear power plants. Nuclear reactor and turbine buildings locate on flat land constructed by excavation, leaving these slopes. In earthquake-resistant design of plants, it is necessary to examine slope stability and, in the worst case, the effect of the downward collapse of soil on the safety of these buildings.

2.7.4 Measures Against Tsunamis

The safety of nuclear power plants against tsunamis is examined with the following constraints:

(i) No seawater flows into the site, even at high tide. That is, the height of the site is higher than that of full tide plus the assumed tsunami height.
(ii) Even if the sea surface is lowered during the receding water stage of a tsunami, water intake should be ensured. However, if this intake becomes impossible, cooling water should be ensured by its storage in pits and tanks.
(iii) Seabed scouring or soil accretion around the intake gate by a tsunami should be prevented.

The accident at the Fukushima Daiichi Nuclear Power Plant was caused by the first requirement not being satisfied. Although it is critical to determine the anticipated height of tsunamis at nuclear power plants nationwide, it is also important to maintain cooling system functions. For this, emergency power functions should be secured. Countermeasures, such as a stock of spare power generators at high elevations or in watertight chambers, should be taken for post-disaster operation.

At Hamaoka Nuclear Plant in Shizuoka Prefecture, tsunami barrier walls of height above sea level 18 m and 1.6 km length were constructed along the coast (Fig. 2.33). These are for protection against a tsunami caused by an earthquake that has been predicted along the Nankai sea trough. Figure 2.34 shows the tsunami

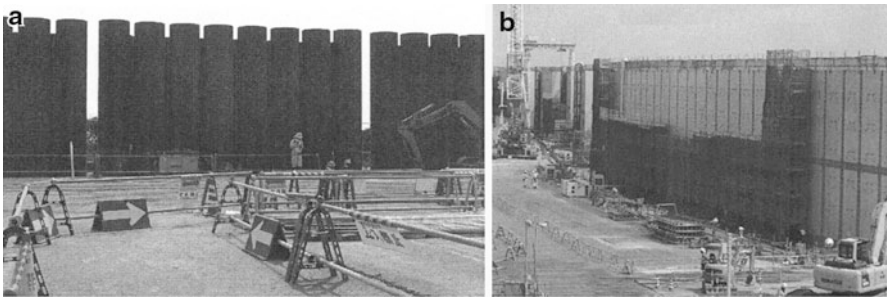

Fig. 2.34 Tsunami barrier wall of Hamaoka nuclear power plant. (**a**) Steel pipe wall. (**b**) Steel box wall

barrier walls under construction, which use continuous steel piles and steel box frames. Construction of such walls is being planned for another nuclear plants. However, the problem for wall design is the tsunami height. Geologic and seismic surveys by the Central Council for Disaster Prevention indicate that tsunamis of several tens of meters height may impact the sea coast along the Nankai Sea trough. In addition to hardware measures including construction of tsunami barrier walls, software measures should be sought to avoid serious accidents. These would maintain electric power source systems for cooling, even if tsunami water overtops barrier walls and flows into the site.

2.8 Countermeasures for Sewage Facilities Against Tsunamis

In the 2011 Tohoku earthquake, wastewater treatment plants and pumping stations of sewage systems were subjected to severe damage across a wide region, from the Tohoku to the Kanto. Among these plants within an area 100 m from the coast, 90 % lost all function. Furthermore, with tsunami inundation height greater than 3.0 m, all wastewater treatment function ceased. To deal with such damage to sewage systems from tsunamis, the Technical Committee for Earthquake and Tsunami Restraint Sewage Systems proposed a basic concept for design and countermeasures of sewage facilities against tsunamis [18]. In this proposal, prevention of wastewater backflow, pumping, and disinfection were designated as mandatory functions. Functions of sedimentation and sludge treatment should be rapidly recovered, although temporary interruptions were allowed. Facilities with the mandatory functions should be located above inundation water levels, or be protected by walls of height greater than those levels (Fig. 2.35). For facilities whose functions should be rapidly recovered, water protection structures are required.

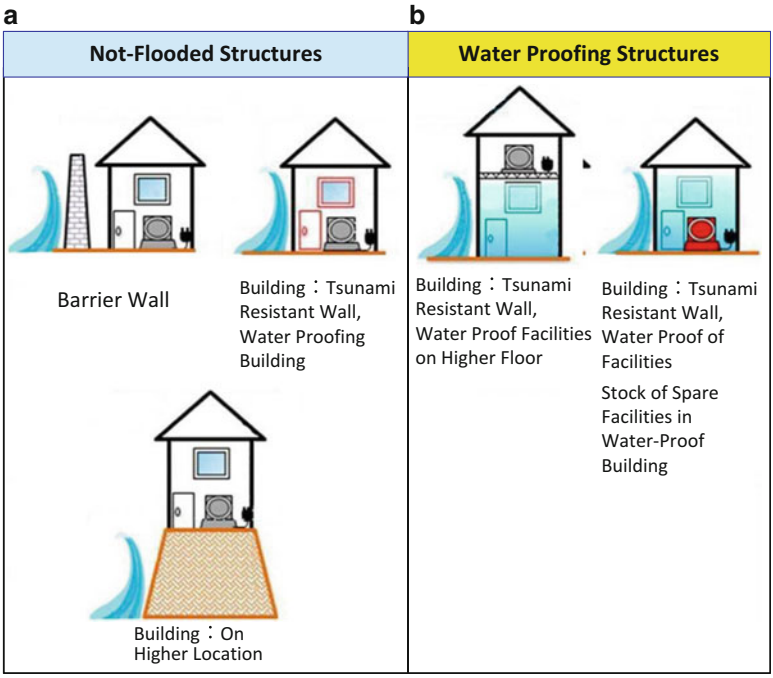

Fig. 2.35 Measures for sewage system against tsunami. (**a**) Measures for preservation of function. (**b**) Measures for quick recovery of function

When sewage facilities are severely damaged by earthquake ground motion or tsunami, the impact on the public is severe. There is the possibility for a secondary disaster, such as the spread of disease. All of treatment plants and pumping stations are built on sites near coasts. Therefore, both hardware and software measures should be implemented. The latter include the security of emergency electric power sources and evacuation system for the staffs.

References

1. Sano R (1917) Theory of earthquake resistant structures of houses, Association for Earthquake Disaster Prevention
2. National Research Institute for Earth Science and Disaster Prevention Home Page. http://www.bosai.go.jp/e/
3. Japan Road Association (1996/2002) Specifications for highway bridges, and explanation, Part V Seismic design. Japan Society of Civil Engineers (JSCE) (2000) Earthquake resistant codes in Japan, 1996 Seismic design specifications of highway bridges
4. JSCE (1965) Report on the 1964 Niigata earthquake and the caused damage (in Japanese)
5. Duke CM, Moran DF (1975) Guideline for evolution of lifeline earthquake engineering. In: Proceedings of the US national conference on earthquake engineering

6. Japan Gas Association (1982) Standards for earthquake resistant design of high pressure gas (in Japanese)
7. Nishi H, et al. Calculation of overflow volume of oil due to sloshing vibration, Journal of Pressure Technology, no. 46, vol. 5, pp 276–284 (in Japanese)
8. JSCE (1996) Proposal on earthquake resistant for civil engineering structures
9. Cabinet Office of the Japanese Government (1995) Basic disaster prevention plan (in Japanese)
10. Japan Water Works Association (1997) Basic principles of seismic design and construction for water supply facilities/JSCE (2000) Earthquake resistant codes in Japan
11. Railway Technical Research Institute (1999) Seismic design for railway structures and commentary. Seismic design of railway structures/JSCE (2000) Earthquake resistant design codes in Japan
12. Bureau of the Ports and Harbors, Ministry of Transport (1999) Technical standards and commentaries for port and harbor facilities earthquake resistant design of port facilities/ JSCE (2000) Earthquake resistant design codes in Japan
13. Tokyo Bureau of Waterworks (1212) Report on seismic reinforcement of Murayama Reservoir Dam (in Japanese)
14. Hakuno M, Fujino Y, Katada T (1978) Report on the 1978 Izu-shima offshore earthquake and it's caused damage. Bulletin of Seismology Institute University of Tokyo, vol 53 pp 1101–1133 (in Japanese)
15. Morishige R (1970) Special construction works of the Sanyo Shinkansen. Report on design of railway structures (in Japanese)
16. Hatton JW, Forster PF, Thomson R (1991) The influence of foundation conditions on the design of Clyde Dam Trans. 17 ICOLD (17th international commission on large dams), vol 66
17. Nuclear Safely Committee (2006) Safely guidelines for earthquake resistant design of nuclear power plant (in Japanese)
18. Technical Committee for Earthquake and Tsunami Resistant Sewage Systems (1212) Japan Sewage Works Association. Basic concept for design and countermeasures of sewage facilities against tsunamis (in Japanese)

http://www.springer.com/978-4-431-54891-1

Engineering for Earthquake Disaster Mitigation
Hamada, M.
2014, XIX, 328 p. 354 illus., 117 illus. in color.,
Hardcover
ISBN: 978-4-431-54891-1